THE EUROPA-MODELL OF THE DEUTSCHER WETTERDIENST

Detlev Majewski
Deutscher Wetterdienst
Offenbach a.M., Germany

1. INTRODUCTION

To meet the growing demand of the public for accurate and detailed weather forecasts, the national meteorological services are developing high-resolution numerical weather prediction (NWP)-models.

Basically, three alternatives exist (see Tab. 1) each of which has intrinsic advantages and disadvantages. The first method requires vast computer resources usually not available at national centers. A global model with uniform resolution of some 15 km may still be some years away even at ECMWF and would be a very inefficient and costly solution of the problem anyway. The variable resolution approach of e.g. France may be an attractive alternative if the crucial dependence of parameterization schemes on mesh size can be overcome. But even this method is rather costly and, if implemented in a spectral model, will require rather large streching factors for a proper representation of orography which is an important forcing on the mesoscale.

As of now, most countries rely on the third solution, the implementation of a model chain. This method makes the best use of available computer resources but has the potential disadvantage of costly maintenance. For example at Deutscher Wetterdienst (DWD), two separate groups are responsible for maintaining the large-scale Global-Modell (GM) and the meso-α-scale Europa-Modell (EM). A third group is developing a meso-ß-scale model (Deutschland-Modell, DM at DWD) in close cooperation with the Swiss Meteorological Agency (SMA). This model is based on the EM-code at present, but will need much more development work before the operational implementation scheduled for 1993. If communication between these three groups (four, including the SMA) does not work properly, inefficient use of the available manpower will certainly result. The two former methods are free from these problems because only one model code has to be maintained. With the "Unified Model", the UK Met. Office tries to overcome this difficulty of the model chain by developing one single code for the global and regional model version.

From the theoretical point of view, the artificial lateral boundaries of the regional model form the most critical disadvantage of such models. Present practical experience at several national centers, however, suggests that a simple one-way-influence nudging method with frequent updating of the boundary values in a marginal zone is an efficient and robust way to overcome this problem.

2. DESCRIPTION OF THE MODEL

The Europa-Modell (EM) is the main weather forecast model of the new numerical weather prediction system of the Deutscher Wetterdienst, which became operational on 15 January 1991. Currently, this system consists of the global spectral model (GM) for large-scale predictions, and the regional model EM for the synoptic and meso-α-scale. A high-resolution meso-ß-scale model for Germany will be added in 1993.

The main goals of EM are:

- more detailed forecasts of weather parameters close to the ground and a better simulation of clouds and precipitation,
- the preparation of meteorological fields for environmental applications, e.g. modeling of air pollution or sea state,
- to serve as a research tool.

2.1 Governing equations

EM is based on the primitive equations in a terrain-following hybrid coordinate system. The prognostic variables are:

- surface pressure p_s ,
- horizontal wind components (u, v),
- total heat $h = c_p T + L q_v$, defined as the sum of enthalpy and latent heat of condensation,
- total water content $q_w = q_v + q_c$, which is the sum of the specific content of water vapor q_v and cloud water q_c.

Assuming water saturation in clouds, the three variables temperature T, water vapor content q_v, and cloud water content q_c can be determined diagnostically from the prognostic variables h and q_w distinguishing between cloud and no-cloud cases.

Type of model	Advantages	Disadvantages
Global model with uniform resolution (ECMWF)	Maintenance "Constant" mesh size	Computational costs Highly inefficient
Global Model with variable resolution (France)	Maintenance Flexibility	Parametrization Inefficient
Model chain (FRG, France, HIR-LAM, Japan, UK, USA)	Very efficient Local data bases	Maintenance Lateral boundaries Graphics, follow-up models

Tab. 1 High-resolution NWP-models - Three alternatives

The five prognostic and ten diagnostic equations which form the relations of the moist atmosphere are given in the Appendix.

2.2 Model domain

The integration area of EM covers the North Atlantic and Europe with a mesh of 181*129 grid points (mesh size 0.5°) in rotated spherical coordinates (Fig. 1). The rotated north pole has the geographical coordinates λ = 170°W and φ = 32.5°N. In this coordinate system, the domain extends from φ' = 32°S to 32°N where the convergence of the meridians is still small. Thus, the true distance between grid points in W-E-direction varies only between 55.6 km in the center of the domain and 47.1 km at the southern and northern edges; in N-S-direction, the distance is 55.6 km.

2.3 Topography

For each 0.5° * 0.5°-grid box several topographic parameters are defined:

- mean height above sea level,
- portion of box covered by land,
- prevailing soil type,
- vegetation cover,
- roughness length over land.

The first two parameters are derived from a 10'*10'-data set (Navy-tape); the third from FAO/UNESCO-maps (1971-78); the fourth is currently set to 0.75 over land not covered by ice or rock. The last parameter depends on the land use and the subgrid-scale variation of orography. The albedo depends on soil type, snow coverage, and soil wetness. Sea ice will be analyzed daily by the winter 1991/1992 using digitalized ice maps.

Fig. 2a shows the mean height above sea level (orography, unit: m) for a portion of the EM-grid covering Central Europe.

2.4 Vertical structure

In the vertical, the atmosphere is resolved by 20 layers of upward increasing thickness in a hybrid coordinate system (Fig. 3a). Eight layers are used in the lowest 2 km of the atmosphere to reproduce the structure of the boundary layer sufficiently well; four

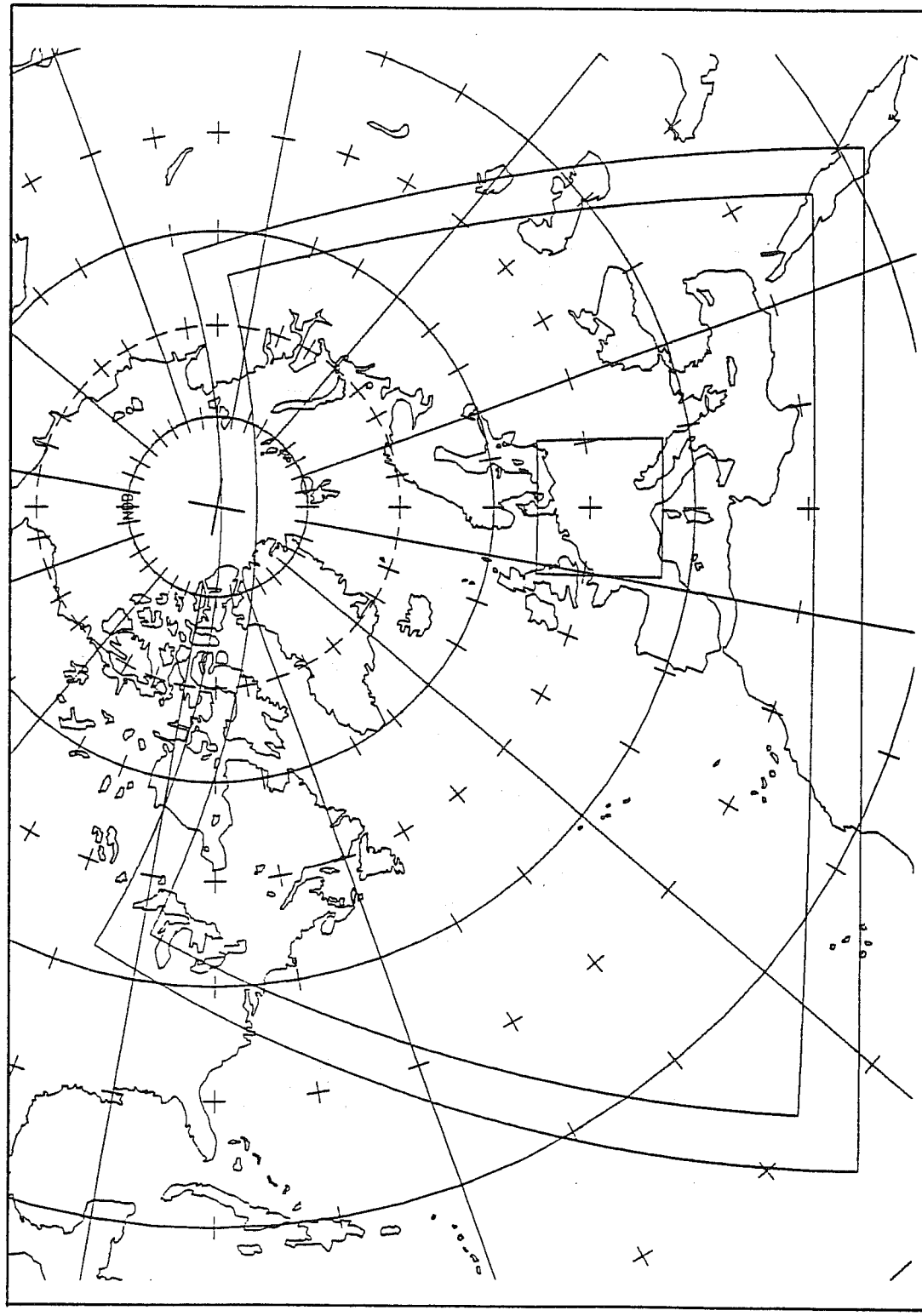

Fig. 1 Domain of Europa-Modell (EM) including the boundary zone and the domain of the future Deutschland-Modell (DM).

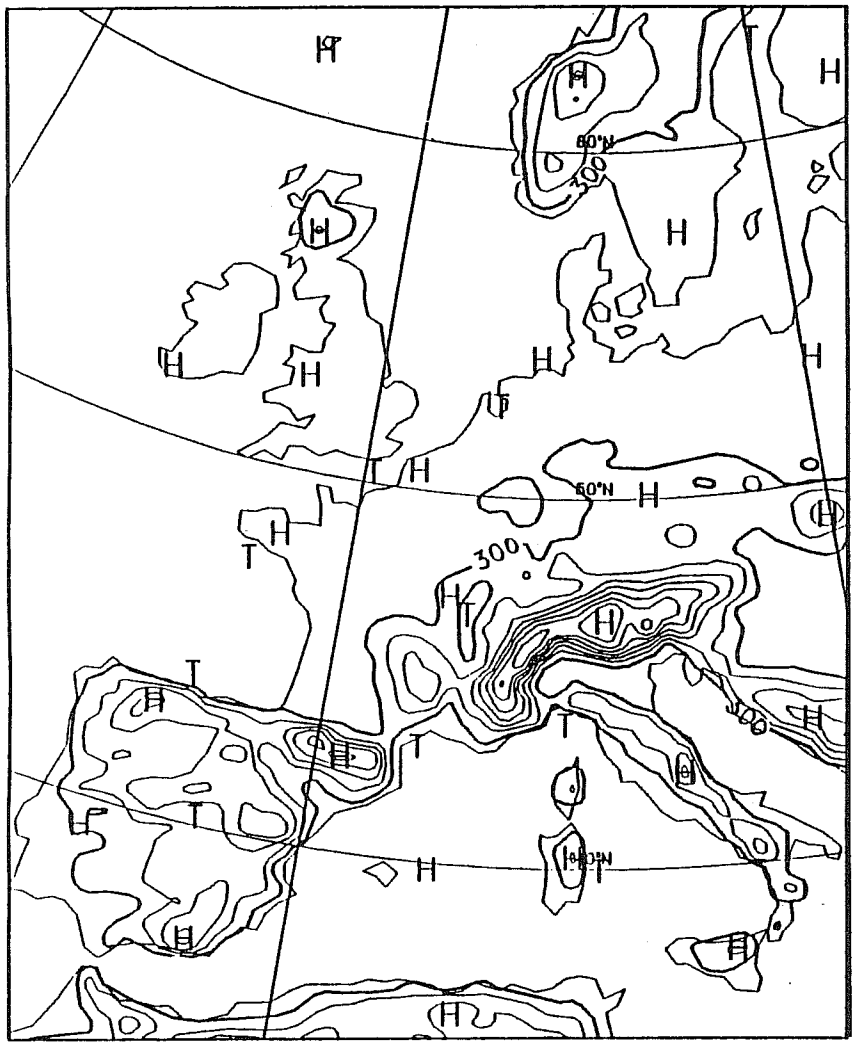

Fig. 2a Orography of Europa-Modell (EM) for Central Europe.

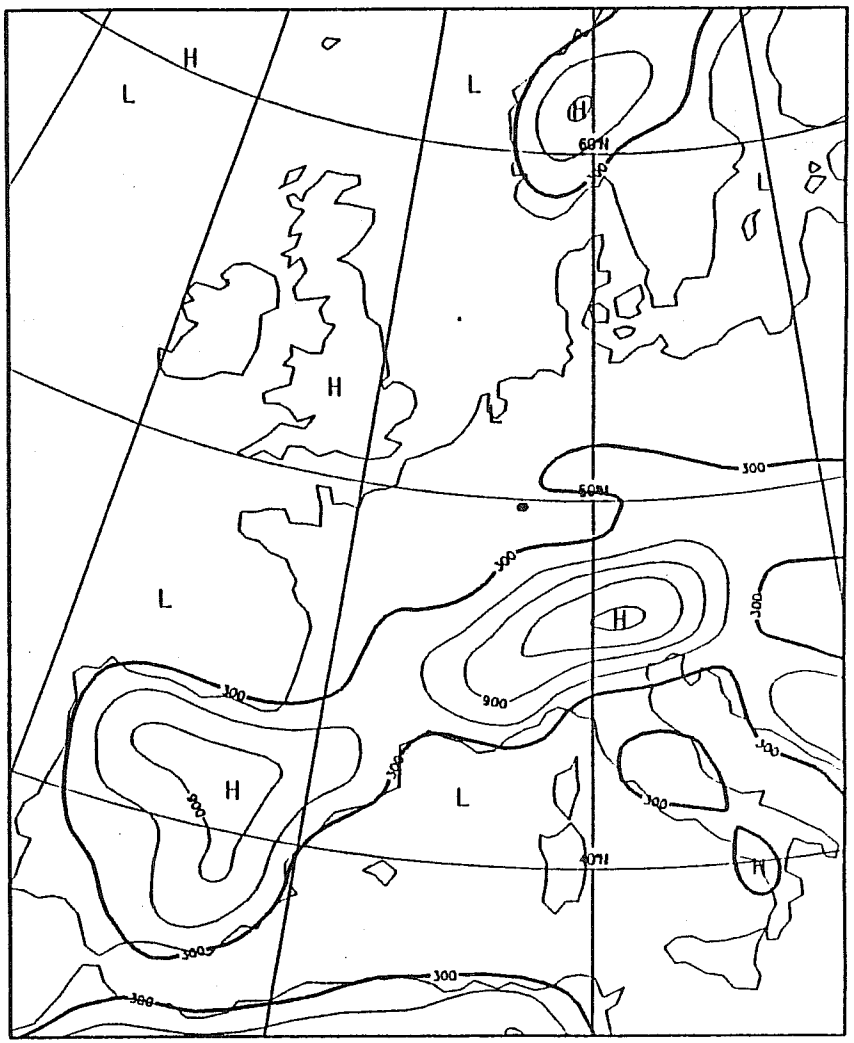

Fig. 2b Orography of Global-Modell (GM) for Central Europe.

Reference line: 300 m; increment 300 m.

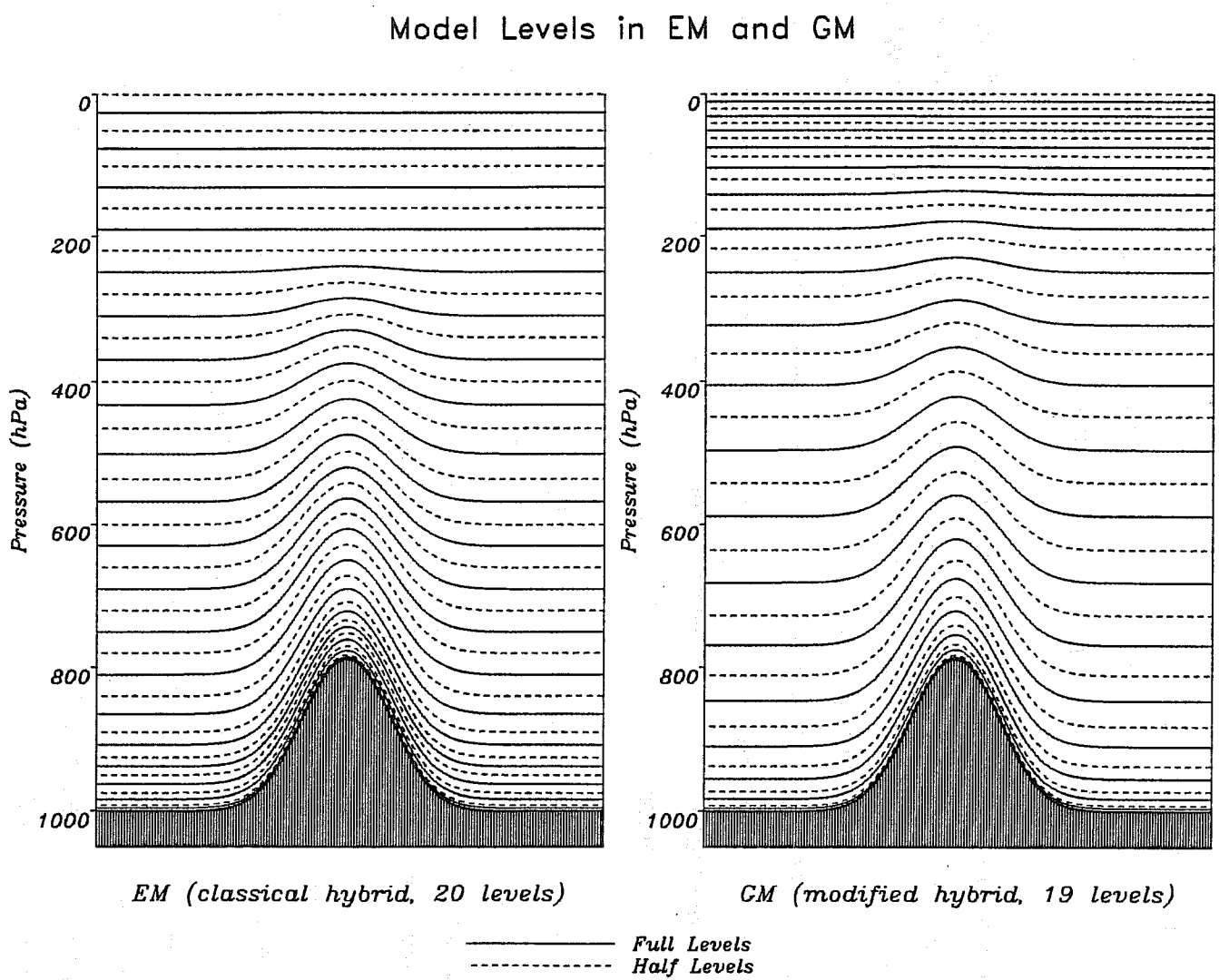

Fig. 3 Model levels of the Europa-Modell (EM) and Global-Modell (GM)

layers are placed in the stratosphere. The prognostic variables (u, v), h, and q_w as well as the diagnostic quantities T, q_v, q_c, and ω, the vertical velocity in the pressure system, are defined at the center of the layers (full levels). The geopotential (Φ), the vertical velocity in the hybrid system ($\dot{\eta}$), and the vertical diffusive fluxes are evaluated at the layer interfaces (half levels).

2.5 Boundary conditions

At the top ($\eta = 0$) and the bottom ($\eta = 1$) of the atmosphere, the vertical velocity ($\dot{\eta}$) vanishes because there is no mass flux across these boundaries.

At the lateral boundaries, time-dependent boundary values for all prognostic variables at an interval of three hours are provided by a run of the Global-Modell (GM) from the same initial date as EM. GM is the ECMWF-model (currently cycle 34 at DWD) with spectral truncation T106 and 19 vertical levels (Fig. 3b). Presently the main difference between GM and the ECMWF-model is the orography, which is a mean one for GM and an envelope-type one at ECMWF. Fig. 2b shows the orography of GM (Gaussian grid of resolution 1.125°) for Central Europe. The maximum height of the Alps is only around 1500 m for GM, whereas the barrier extends to a height of up to 2300 m in EM.

Special care is taken to interpolate the GM-fields smoothly onto the EM-grid and adapt them to the EM-orography (Majewski, 1985). The relaxation scheme after Davies (1976) is used which adjusts the prognostic variables in a marginal zone of 8 grid rows towards the prescribed GM-fields. There is no influence by EM on the GM-forecast.

2.6 Numerical schemes

The prognostic equations are written in advective form on an Arakawa C-grid. Second order central differences in space are used. The vertical finite difference formulation conserves energy and angular momentum (Simmons and Burridge, 1981). Time stepping is leap-frog with semi-implicit correction and Asselin-filter; the time step is 5 min. Vertical advection and the vertical turbulent fluxes are treated implicitly to avoid numerical instability.

2.7 Physical parameterizations

2.7.1 Horizontal diffusion

The horizontal diffusion of momentum, total heat and water content is second order with a space-dependent diffusion coefficient proportional to the total deformation of the horizontal wind field. The coefficients are in the range of 10^4-$10^6 m^2/s$. Horizontal diffusion is performed on the hybrid levels but correction terms are added in the heat and moisture equations to account for the slope of the model layers.

2.7.2 Vertical turbulent fluxes

In the Prandtl layer, the Dyer-Businger relations as modified by Louis (1979) are used. In the Ekman layer and the free atmosphere, a second order closure scheme of hierarchy level 2 (Mellor and Yamada, 1974) has been developed. The exchange coefficients depend on the stability, the wind shear, and the horizontal diffusion coefficients. The roughness length over water is computed according to Charnock. The whole turbulent scheme is described in detail by Müller (1981).

Fig. 4a shows the drag coefficients for momentum and heat as a function of the Richardson number. Fig. 4b presents the diffusion coefficients in the atmosphere.

2.7.3 Soil model

If the land portion of a grid box is less than 50 %, this grid point is treated as sea point whose temperature is kept constant during the forecast. The temperature is provided by a sea surface temperature (SST) analysis.

For land points a soil model predicts the temporal evolution of temperature and water content. The soil model comprises two layers in the soil (about 10 cm and 25 cm, depending on soil type, for the heat budget; 10 cm and 90 cm for the water budget) and a variable storage at the surface for the interception of water or snow. Climatological values are prescribed below these layers. The heat budget is formulated according to the extended force-restore method (Jacobsen and Heise, 1982). No analysis of the soil temperatures and water contents is performed at present, the 6h-first guess of the 4dim. data assimilation (Chapter 2.8.1) is used instead.

2.7.4 Grid-scale precipitation

The parameterization of the cloud microphysics accentuates the role of the ice phase for precipitation formation by emphasizing the Bergeron-Findeisen process. The

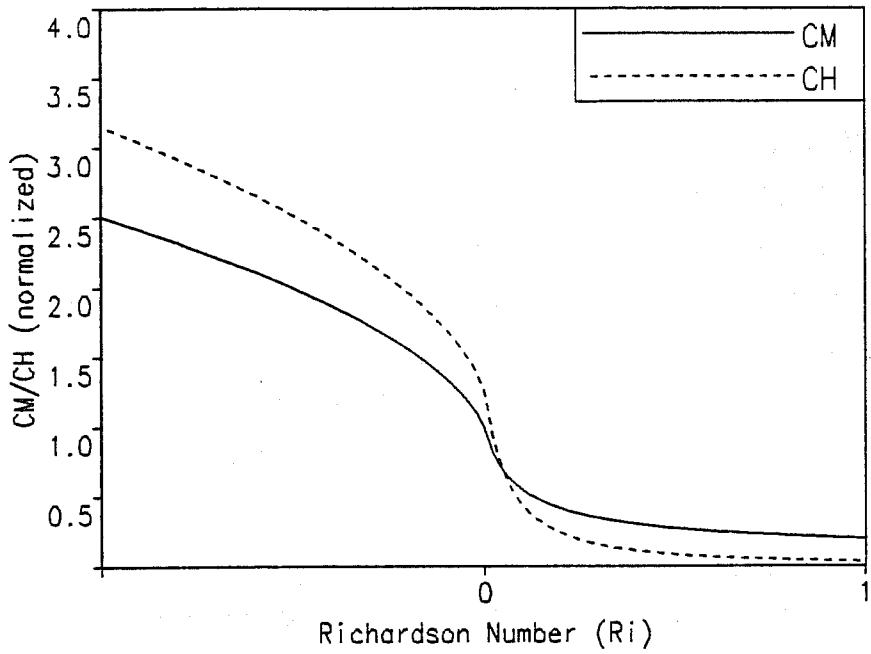

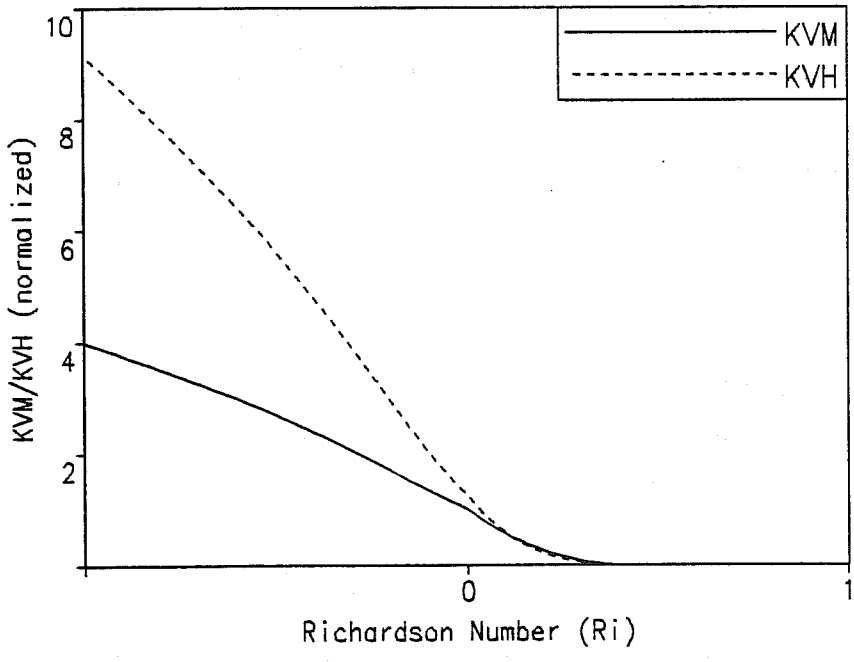

Fig. 4a Normalized drag coefficients for momentum (CM) and heat/moisture (CH) as a function of the Richardson number.

Fig. 4b Normalized diffusion coefficients for momentum (KVM) and heat/moisture (KVH) as a function of the Richardson number.

parameterization scheme is of Kessler-type and allows for interactions between water vapor, cloud water, rain and ice including autoconversion of cloud water to rain and to ice, accretion, riming, shedding, melting, deposition, and evaporation of raindrops. Rainfall and snowfall rates are derived diagnostically assuming stationarity and neglecting advection.

2.7.5 Moist convection

At present a simple soft adjustment scheme is used for the parameterization of moist convection. The reference profiles for h and (u, v) between cloud base and top are the pressure weighted vertical averages of moist static energy and (u, v). The reference profile for q_w on the whole corresponds to 60 % of the saturation value scaled by the actual humidity content between cloud base and top. A time constant of 1 hour is chosen. Resulting liquid water falls out immediately and is defined as rain or snow depending on temperature. Evaporation of precipitation in subsaturated layers is taken into account.

The soft adjustment scheme will be replaced by a more sophisticated mass-flux scheme by the summer of 1992.

2.7.6 Cloudiness and radiation

In saturated layers ($q_c > 0$) 100 % cloudiness is assumed and the liquid water content q_c is used in the evaluation of radiative fluxes. In subsaturated layers ($q_c = 0$) a fractional cloud cover is derived from relative humidity and its liquid water content set to 1 % of the saturation value.

The computation of solar fluxes takes into account the effects of Rayleigh scattering, absorption and scattering by clouds and aerosol, and absorption and reflexion by the ground. Longwave radiation fluxes are influenced by the vertical profiles of temperature, water vapor, trace gases, and clouds.

25 % of the CP-time for an EM-forecast is spent in the radiation scheme, even though a full radiation step is performed only every 1.5 hours.

The radiation scheme will be replaced by an improved version by the summer of 1992. Presently the new scheme is tested in GM.

2.7.7 Mean energy and water fluxes in EM

The parameterized physical processes control to a large extent the model climate. Fig.5 gives an overview of the monthly mean energy and water cycle of EM consisting of all 00 UTC-forecasts up to 72 hours for July 1991. The fluxes are integrated over the full domain of EM (Fig. 1) which consists of 44 % land and 56 % water points. Shown here are the radiation balance of short- and longwave fluxes at the top and the bottom of the atmosphere and the turbulent fluxes of momentum, heat, and water vapor at the surface; also precipitation (rain and snow) as well as total cloudiness.

2.8 Operational suite

In the operational environment we have to distinguish between data assimilation and forecast.

2.8.1 Data assimilation

Fig. 6 shows schematically the intermittent 4-dimensional data assimilation streams for GM and EM. These two streams proceed in parallel and are coupled only via the boundary data written by GM every 3 hours. A 6h-EM-forecast provides the first guess fields for the EM-analysis inside the EM-domain; the corresponding 6h-GM-forecast augments the fields in a 10°-wide zone around the EM-area. The limited-area version of the multivariate OI-analysis scheme of GM (Lorenc, 1981) takes into account all available observations in a 6h-window centered around the analysis times 00, 06, 12, and 18 UTC. To allow for observations arriving very late, the cut-off times of the assimilation analyses are as late as possible (see Tab. 2). Presently the correlation functions used in the OI-scheme of the EM-analysis are based on modified GM-values. In the near future, EM-first guess error correlations will be derived to improve the EM-analysis especially in the meso-α-scale.

After the analysis an implicit nonlinear normal mode initialization (INMI, Temperton, 1988) is performed to balance the EM mass and wind fields. Two iterations for the first three modes are sufficient to remove high frequency gravity oscillations.

The cold start of the GM- and EM-assimilation was on 12 September 1990 and no new cold start was necessary since then.

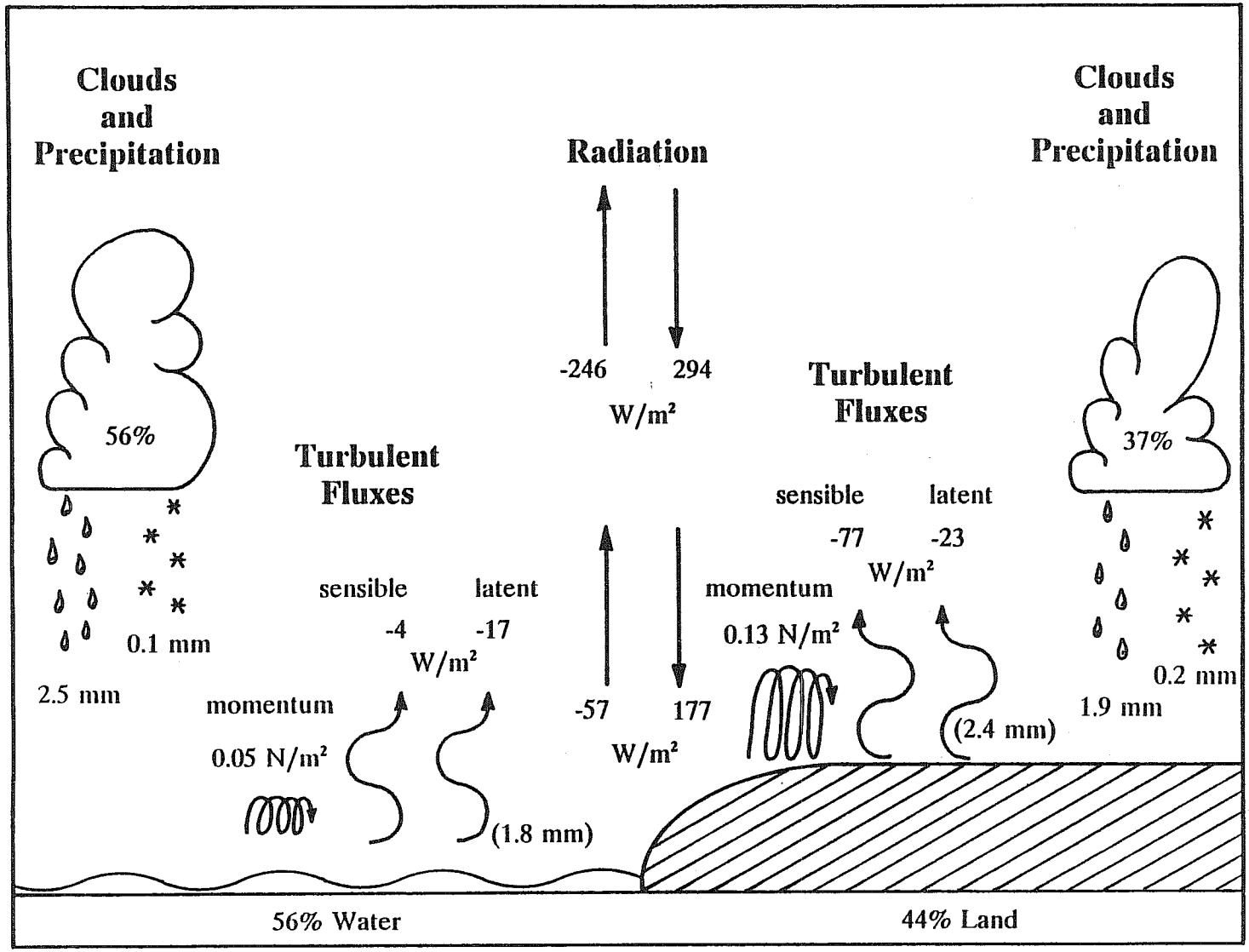

Fig. 5 Components of the energy and water cycle of EM.
Mean of all 00 UTC-forecasts up to 72h for July, 1991.
Area mean over full domain, for land and sea points separately.

Start	End	Product			
0031	0054	Final analysis of yesterday	12 UTC;	GM and EM	(ASS)
0054	0114	6h-forecast valid yesterday	18 UTC;	GM and EM	(ASS)
0115	0140	Final analysis of yesterday	18 UTC;	GM and EM	(ASS)
0140	0200	6h-forecast valid today	00 UTC;	GM and EM	(ASS)
0215	0224	Analysis of today	00 UTC;	GM	(PRE)
0228	0300	36h-forecast starting today	00 UTC;	GM	(PRE)
0330	0353	Analysis of today	00 UTC;	GM and EM	(MAIN)
0355	0625	168h-forecast starting today	00 UTC;	GM	(MAIN)
0405	0535	78h-forecast starting today	00 UTC;	EM	(MAIN)
1231	1254	Final analysis of today	00 UTC;	GM and EM	(ASS)
1254	1314	6h-forecast valid today	06 UTC;	GM and EM	(ASS)
1315	1340	Final analysis of yesterday	06 UTC;	GM and EM	(ASS)
1340	1400	6h-forecast valid today	12 UTC;	GM and EM	(ASS)
1415	1424	Analysis of today	12 UTC;	GM	(PRE)
1428	1500	36h-forecast starting today	12 UTC;	GM	(PRE)
1530	1553	Analysis of today	12 UTC;	GM and EM	(MAIN)
1555	1825	168h-forecast starting today	12 UTC;	GM	(MAIN)
1605	1735	78h-forecast starting today	12 UTC;	EM	(MAIN)

GM: Global-Modell; EM: Europa-Modell; ASS: Assimilation;
PRE: Forecasts with very short cut-off; MAIN: Main forecast.

Tab. 2 Operational schedule of assimilation and forecasts at DWD

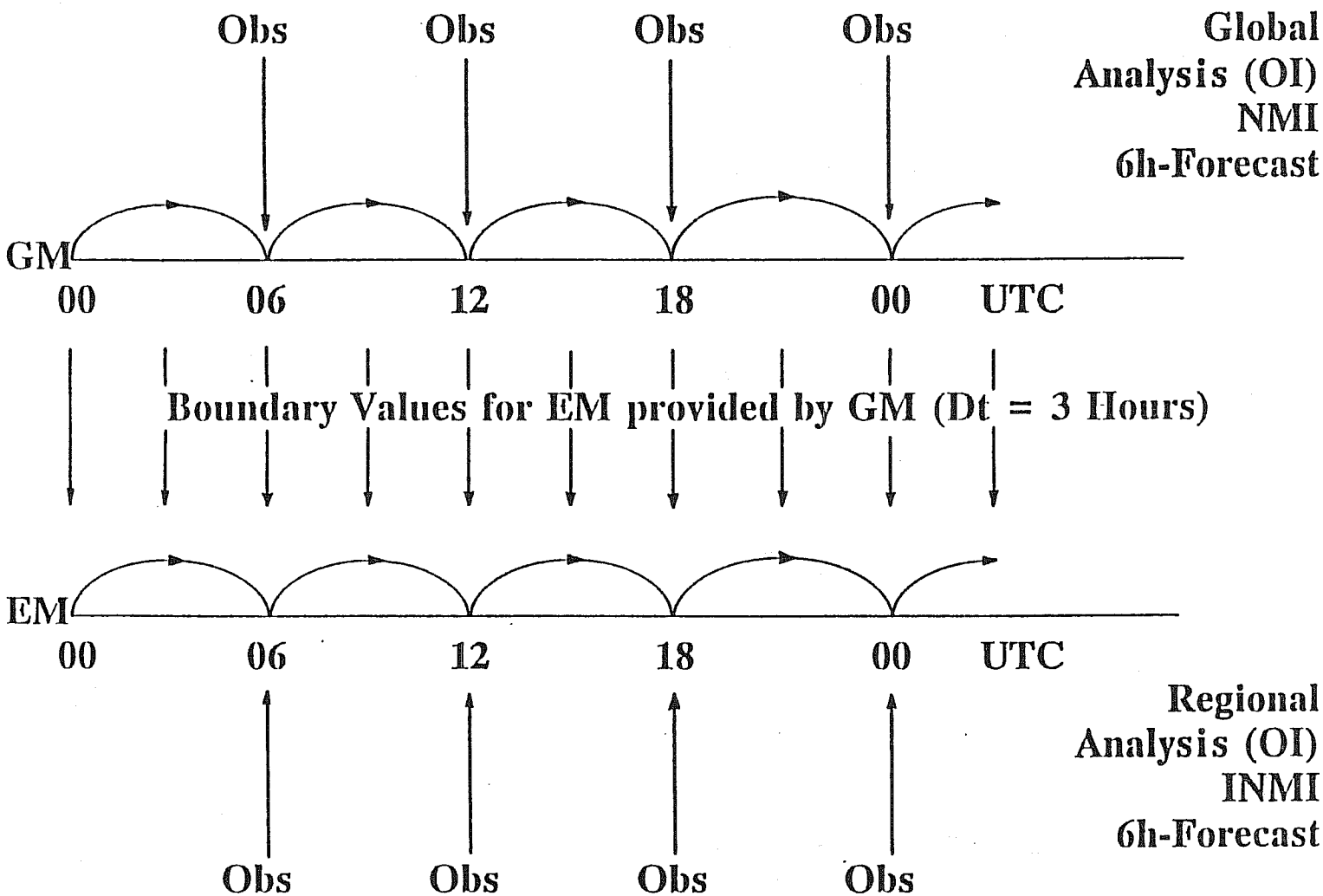

Fig. 6 4Dim. data assimilation for GM and EM.

2.8.2 Forecasts

78h-EM-forecasts are produced twice a day (see Tab. 2) for 00 and 12 UTC with a short cut-off time of 3h 26min. The boundary data for these forecasts are provided in 3h-intervals by a GM-run from the same initial date. Thus EM gets the best possible lateral boundary conditions available.

Two additional 36h-GM-forecasts with a very short cut-off time of 2h 11min allow early numerical guidance to be given.

2.9 Available products

All EM-analysis and forecast fields are stored in Grib-code (FM 92-VIII). Archiving on tapes started in May 1991.

The following parameters are available as analysis (A), initialized analysis (IA) and forecasts. Analysis and initialized analysis are available daily for 00, 06, 12, and 18 UTC. Forecasts are available for the full domain (181 * 129 grid points, 20 levels, index FC) from +6h up to +78h with an increment of 6h; for an area covering Germany and its surroundings (31 * 30 grid points, index D) from +1h up to +78h with an increment of 1h. Additionally the horizontal winds (20 levels) and the surface pressure are stored in 2h-intervals for trajectory computations and wave modeling.

2.9.1 Multi-level fields on the 20 hybrid model-levels

	Name of field	Unit	Availability
U	wind component in λ'-direction	m/s	A, IA, FC, D
V	wind component in φ'-direction	m/s	A, IA, FC, D
FI	geopotential	gpm	A, IA, FC, D
T	temperature	°C	A, IA, FC, D
QV	specific humidity content	kg/kg	A, IA, FC, D
QC	specific cloud water content	kg/kg	A, IA, FC, D
OMEGA	vertical velocity (dp/dt)	hPa/s	IA, FC, D

2.9.2 Multi-level fields on pressure levels

Currently fields on the following pressure levels are available:

50, 100, 200, 250, 300, 400, 500, 700, 850, 950, 1000 hPa.

The fields on pressure levels are derived by vertical interpolation of model level fields using tension splines. Also a slight horizontal smoothing by digital filters is performed.

	Name of field	Unit	Availability
U	wind component in λ'-direction	m/s	A, IA, FC, D
V	wind component in φ'-direction	m/s	A, IA, FC, D
FI	geopotential	gpm	A, IA, FC, D
T	temperature	°C	A, IA, FC, D
RH	relative humidity	%	A, IA, FC, D
OMEGA	vertical velocity (dp/dt)	hPa/s	IA, FC, D

Additionally the mean sea level pressure is available (A, IA, FC, D).

2.9.3 Single-level fields

Topographic fields that do not change with time are stored only once. At present, there are five constant fields:

	Name of field	Unit	Availability
FIB	orography	gpm	constant
BLA	portion of grid box covered by land (between 0 and 1)	-	constant
BTY	soil type (number between 1 and 9)	-	constant
PHI	geographic latitude	Deg.N	constant
RLA	geographic longitude	Deg.E	constant

Some fields remain constant during the forecast but change climatologically. These fields are only available as analyses.

Name of field		Unit	Availability
TU	climatic deep soil temperature	K	A
WU	climatic deep soil water content	m H_2O	A
VIO3	ozone content (vertical integral)	Pa (O_3)	A
HMO3	height of ozone maximum	Pa	A

All other fields change with time.

Name of field		Unit	Availability
PS	surface pressure	hPa	A, IA, FC, D
TS	temperature of snow surface (or surface temperature)	K	A, IA, FC, D
TB	temperature below snow (or surface temperature)	K	A, IA, FC, D
TM	temperature between upper and lower soil layer	K	A, IA, FC, D
QDB	specific surface humidity content (for latent heat flux)	kg/kg	A, IA, FC, D
WS	water content of snow	m H_2O	A, IA, FC, D
WB	water content of upper soil layer	m H_2O	A, IA, FC, D
WM	water content of lower soil layer	m H_2O	A, IA, FC, D
TCM	coefficient for turbulent transfer of momentum	-	IA, FC, D
TCH	coefficient for turbulent transfer of heat, water vapor	-	IA, FC, D
SOSB	short wave radiation balance at the surface; mean over forecast	W/m^2	IA, FC, D
SOSO	short wave radiation balance at the top; mean over forecast	W/m^2	IA, FC, D

THSB	long wave radiation balance at the surface; mean over forecast	W/m^2	IA, FC, D
THSO	long wave radiation balance at the top; mean over forecast	W/m^2	IA, FC, D
PAR	photosynth. active radiation at the surface; mean over forecast	W/m^2	IA, FC, D
ALB	surface albedo	-	IA, FC, D
RRSN	rain (grid scale); sum since start of forecast	kg/m^2	IA, FC, D
RSSN	snow (grid scale); sum since start of forecast	kg/m^2	IA, FC, D
RRKN	rain (convective); sum since start of forecast	kg/m^2	IA, FC, D
RSKN	snow (convective); sum since start of forecast	kg/m^2	IA, FC, D
U1OM	wind component in λ'-direction at 10 m above surface	m/s	IA, FC, D
V1OM	wind component in φ'-direction at 10 m above surface	m/s	IA, FC, D
T2M	temperature at 2 m above surface	°C	IA, FC, D
TD2M	dew point at 2 m above surface	°C	IA, FC, D
TMIN2M	minimum temperature during the previous 6 hours at 2 m	°C	IA, FC, D
TMAX2M	maximum temperature during the previous 6 hours at 2 m	°C	IA, FC, D
VBM1OM	maximum wind speed during the previous 6 hours at 10 m	m/s	IA, FC, D
GZO	roughness length	m	IA, FC, D
CLCT	total cloud cover	-	IA, FC, D
CLCH	high cloud cover	-	IA, FC, D
CLCM	medium cloud cover	-	IA, FC, D
CLCL	low cloud cover	-	IA, FC, D
BASINK	base index of main convective cloud	-	IA, FC, D
TOPINK	top index of main convective cloud	-	IA, FC, D
BFLU	momentum flux of u at the surface; mean over forecast	N/m^2	IA, FC, D

BFLV	momentum flux of v at the surface; mean over forecast	N/m^2	IA, FC, D
BFLH	sensible heat flux at the surface; mean over forecast	W/m^2	IA, FC, D
BFLQD	latent heat flux at the surface; mean over forecast	W/m^2	IA, FC, D

3. SOME NUMERICAL ASPECTS OF EM

During the design and implementation of EM, several numerical problems arose which had to be dealt with. The solutions of some of them, which are typical of regional-scale models, are presented in this chapter.

3.1 Efficiency of the semi-implicit time stepping

The choice of a rotated spherical grid for EM is not only advantageous regarding the CFL-time step (see chapter 2.2) but facilitates also a fast solution of the Helmholtz-equations in the semi-implicit (SI) time stepping. Because the Helmholtz-equations in rotated spherical coordinates have no map factor in the "zonal" direction, a direct solver is implemented which consists of a FFT in "zonal" and Gaussian elimination in "meridional" direction of the EM-grid. The equations are solved assuming a vanishing second time-derivative of divergence at the boundaries, which is consistent with the linear interpolation with time of the boundary values provided by GM. The direct solver is approx. four times faster than an iterative multi-grid method for the same number of grid points. The FFT has the minor disadvantage that the necessary factorization limits the choice of the number (IE) of grid points in "zonal" direction of the grid; i.e. $IE\text{-}1 = 2^k \cdot 3^l \cdot 5^m$ (for integer k, l, m) at present.

For EM, the stable explicit time step is 45 s while the semi-implicit time step is 300 s. If the SI-scheme did not require extra computational efforts, a speed-up of EM by a factor of 6.67 would be possible. Because of the efficient implementation of the SI-scheme, including the use of special matrix manipulation routines of the Cray-Scilib, a speedup by a factor of 5.09 is realized in practice for the adiabatic model. The speed-up drops to 4.24 if all physical parameterizations are switched on. The reason for the reduced speedup is the costly computation of radiation, which requires 25 % of the computation time and is performed every 1.5 hours of forecast time. Thus the cost of the radiation computation is independent of the time step of EM.

3.2 Implicit treatment of vertical diffusion

To avoid numerical instability, the vertical diffusion terms are treated by the implicit Crank-Nicholson scheme, which is unconditionally stable in the linear case but may not prevent spurious oscillations. G. Doms (1990) discusses the numerical reasons for the oscillatory solutions.

To damp the oscillations, the weight factor ß in the modified Crank-Nicholson scheme

$$\frac{\psi^{n+1} - \psi^n}{\Delta t} = \frac{\partial}{\partial z}\left\{ \beta \left(K_V \frac{\partial \psi}{\partial z}\right)^{n+1} + (1-\beta)\left(K_V \frac{\partial \psi}{\partial z}\right)^{n} \right\} \qquad (1)$$

is set to a value greater than 1; e.g. in the ECMWF-model ß = 1.5. A disadvantage of this approach is that the effective diffusion coefficient is artificially reduced. To confine this reduction to the regions of high vertical resolution close to the ground, where it is necessary to suppress the oscillations, ß varies with height in EM. In the surface layer, ß is set to 1.3, then decreased to 0.75 at a height of 1500 m above ground, and set to 0.75 in the free atmosphere.

Fig. 7 shows the temporal evolution of the 10m-wind speed at a grid point for different values of ß. The wind speed at 10 m is derived diagnostically from the winds at the lowest model level, which is approx. 30 m above ground. The test-version of EM used for these experiments has a mesh size of 1°; thus a CFL time step of 600 s can be used. But with that time step and ß = 0.5, the typical spurious oscillations with a period of 4 Δt develop during the forecast (Curve: E05). If we reduce the time step to 90 s, which is the stable explicit step, the oscillations disappear (Curve: EEX). A smooth evolution will also result if ß is set to 1.5 at all levels (Curve: E15), or chosen height-dependent as in EM (Curve: EM1). The oscillatory behaviour of near-surface parameters can thus be controlled by a very cheap method.

3.3 Implementation of horizontal diffusion

In EM, the horizontal diffusion term F_H^{ψ} in a prognostic equation for a quantity ψ is formulated according to Smagorinsky:

$$F_H^{\psi} = \frac{1}{\rho} \nabla\cdot(\rho K_H \nabla\psi) \qquad with \quad K_H = \frac{(C\Delta)^2}{\sqrt{2}} \, |def| \qquad (2)$$

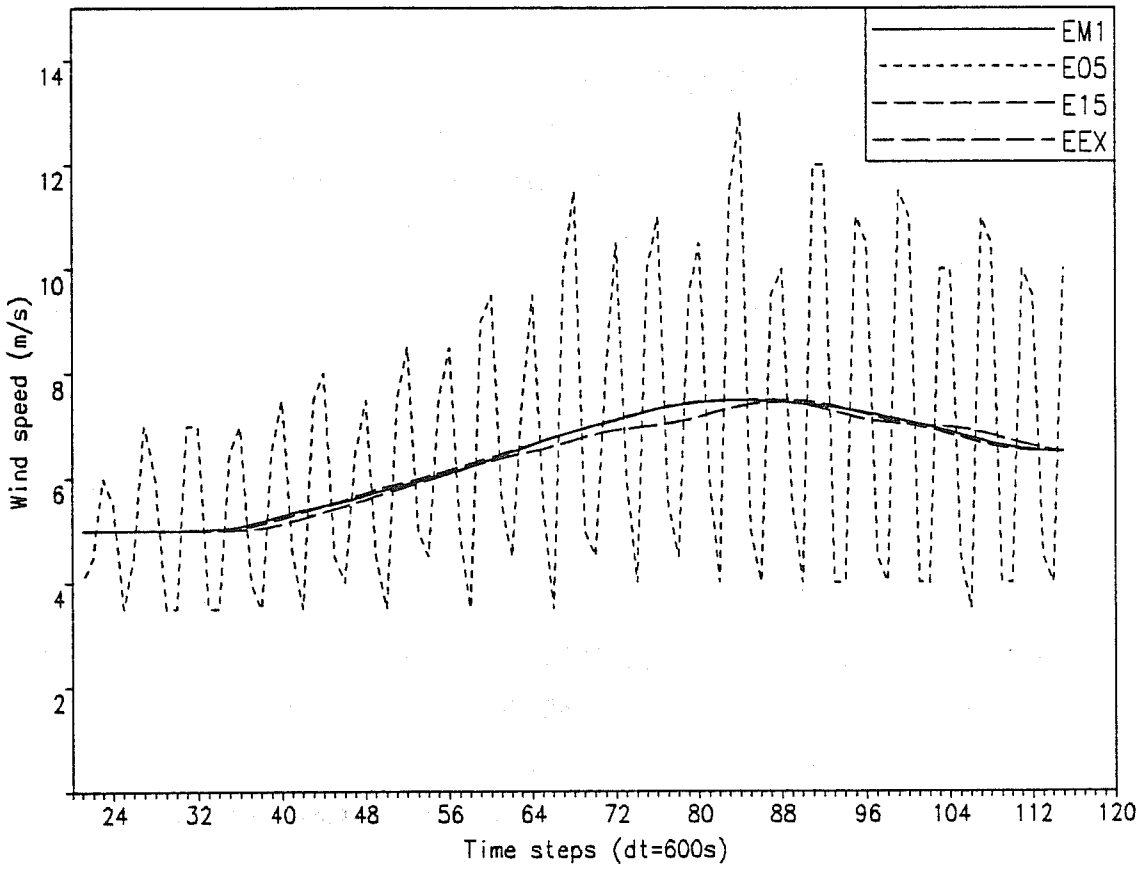

$$\frac{\psi^{n+1} - \psi^{n}}{\Delta t} = \frac{\partial}{\partial z}\left\{ \beta \left(K_V \frac{\partial \psi}{\partial z}\right)^{n+1} + (1-\beta)\left(K_V \frac{\partial \psi}{\partial z}\right)^{n} \right\}$$

Fig. 7 Wind speed at 10m for a grid point over Denmark;
7 Oct. 1987 + 19h.

E05: $\beta = 0.5$, SI-time stepping,
E15: $\beta = 1.5$, SI-time stepping,
EM1: β varies with height, SI-time stepping,
EEX: $\beta = 0.5$, explicit time stepping.

where def is defined by:

$$def^2 = \left(\frac{\partial u}{\partial y} + \frac{\partial v}{\partial x} \right)^2 + \left(\frac{\partial u}{\partial x} - \frac{\partial v}{\partial y} \right)^2 \qquad (3)$$

and includes contributions from shearing and streching. C is a constant and Δ is the mesh width.

However, the diffusion coefficient K_H according to Eq. (2) does not respond properly in areas where strong local grid-scale vertical circulations ("grid point storms") form. These fictitious circulations are associated with large local divergences. Fig. 8a shows the vertical velocity at a grid point over the Mediterranian at a time of strong convective activity which was triggered by switching off the convection scheme of the model. A maximum upward motion of more than -11 Pa/s at 500 hPa is reached. The horizontal diffusion coefficient (Fig. 8b) increases too late and does not prevent the development.

In order to achieve an increased horizontal diffusion at such grid points, the diffusion coefficient is set proportional to the total flow deformation including the dilational part of the velocity field (Doms, 1990). K_H is then defined:

$$K_H = \frac{(C\,\Delta)^2}{\sqrt{2}} \sqrt{def^2 + D^2} \qquad (4)$$

where D is the divergence of the horizontal wind. Fig. 8c and d prove that with the new formulation for K_H, the temporal evolution of the vertical circulations is much smoother and the upward motion has a maximum around -7 Pa/s.

Using a constant K_H of 10^5 m^2/s and a second order linear horizontal diffusion scheme as in Fig. 8e, the grid point storm is only weakly damped and the maximum upward motion is more than -17 Pa/s. Even $K_H = 1.5 * 10^5$ m^2/s is not as efficient as the current EM-scheme in damping the storm (Fig. 8f).

Thus a scheme that includes locally varying diffusion coefficients is better in controlling the development of grid point storms.

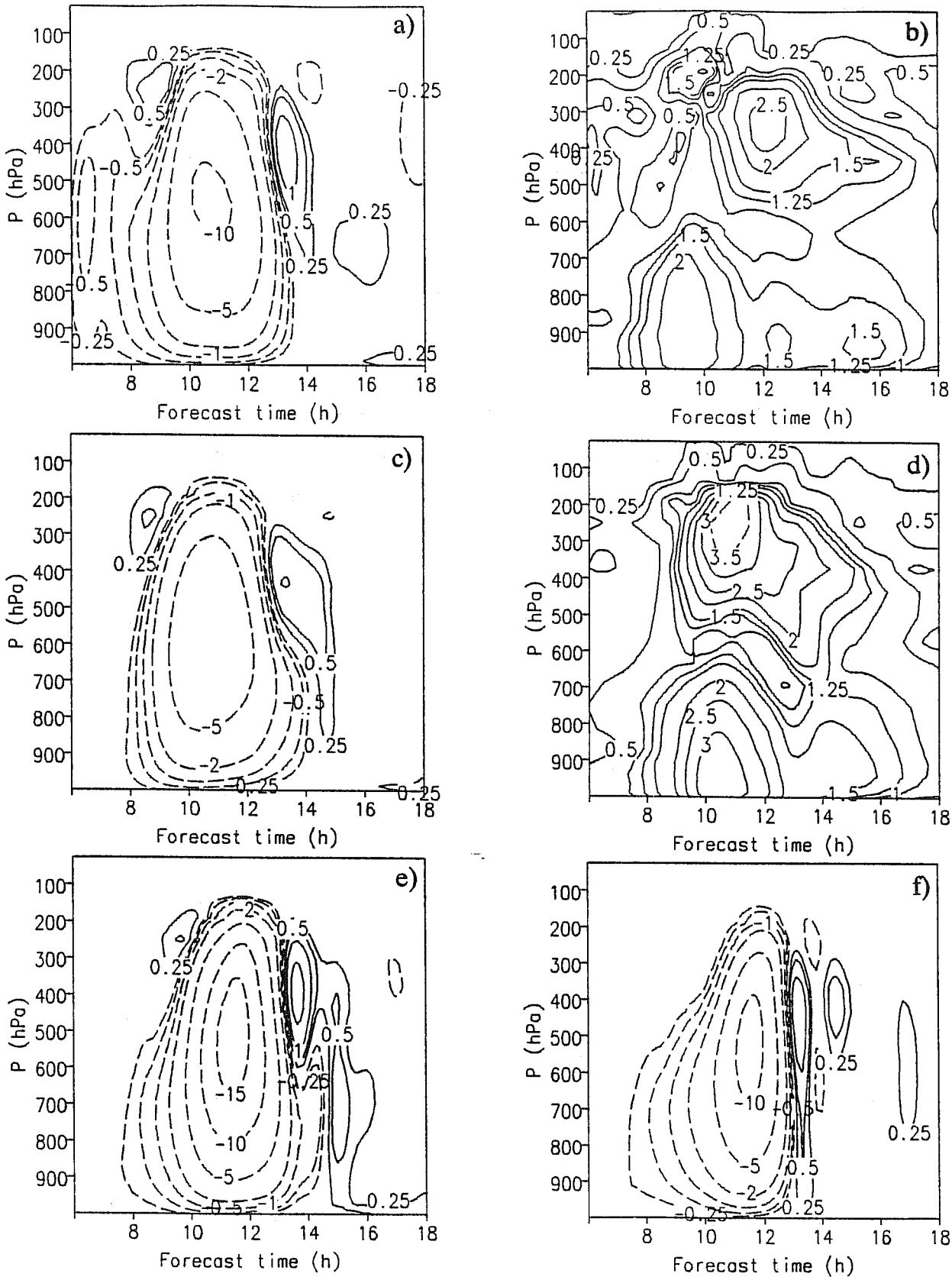

Figs. 8a, c, e, and f: Vertical velocity (Pa/s) at a grid point over the Mediterranian. 7 Oct. 1987 12 UTC + 18h.

Figs. 8b and d: Horizontal diffusion coefficient (10^5 m^2/s) for the same point

3.4 Impact of lateral boundary values

The quality of limited area models is strongly controlled by the available lateral boundary values. For a given driving model two parameters are most important:

- the time lag between the initial dates of the limited-area and driving global model, resp.,
- the update frequency between two write-up times of the boundary values.

Most smaller national meteorological centers have to use boundary values from a global forecast that is already 12 hours old, and have an update interval of six hours at best. In contrast, EM is provided with boundary data from a GM-forecast which is initialized at the same date and time as EM. The update interval of the boundary data is three hours at present and will be reduced to two hours in the near future if disk space becomes available. Majewski (1990) presents an example of the crucial impact of the temporal resolution of boundary data on the forecast quality of the regional model.

For a proper initialization of a limited-area model, the boundary values provided by the driving global model have to be taken into account. In the EM, the implicit nonlinear normal mode initialization (INMI, Temperton, 1988) is used to balance mass and wind fields. To achieve a smooth evolution of the forecast within the boundary zone, the uninitialized EM-analysis is mixed with the initialized GM-analysis of the same date and time, which had been interpolated to the EM-grid and adapted to the EM-orography. To replace the uninitialized EM-fields by the interpolated GM-analysis only at the boundary row of EM is not enough, as Fig. 9 shows for the case of initializing the first three modes with two iterations (Curve: 3M/OR). Mixing both fields in a boundary zone of some eight grid points with a weight proportional to the boundary relaxation coefficients results in a much smoother initial pressure tendency (Curve: 3M/MR). Without initialization (Curve: OI/OR for the case without mixing; curve: OI/MR with mixing), the initial noise in EM is much higher, and six hours of forecast time are not enough to damp it completely.

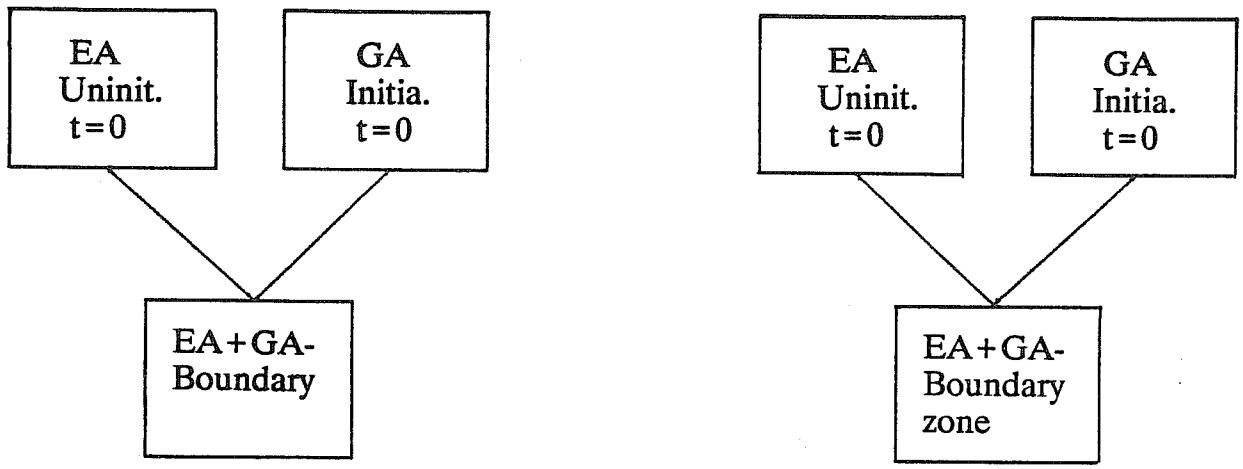

$$\psi^{Mix} = (1 - \sqrt{\alpha})\,\psi^{EA} + \sqrt{\alpha}\,\psi^{GA}$$

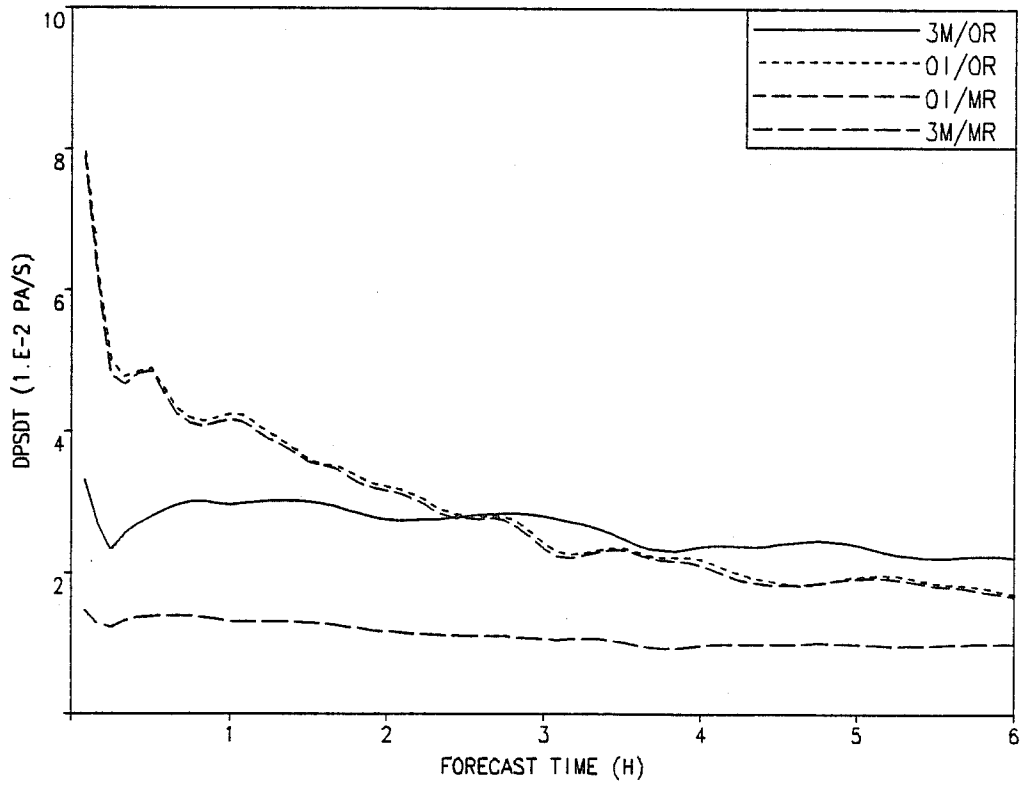

Fig. 9 Area mean of absolute value of surface pressure tendency, 20 Aug. 1991 00 UTC + 6h.

3M/OR: First three modes initialized; EA+GA-boundary,
OI/OR: Without INMI; EA+GA-boundary,
OI/MR: Without INMI; EA+GA-boundary zone,
3M/MR: First three modes initialized; EA+GA-boundary zone.

4. RESULTS AND VERIFICATION

Because EM is being verified systematically at Deutscher Wetterdienst for merely six months, only preliminary results of verification can be presented.

4.1 Difference between EM and GM

Since the GM-fields are transformed to the EM-grid not only for a boundary zone but for the full EM-domain, the difference between EM- and GM-forecasts can be evaluated during the course of the 78h-forecast. As these differences vanish at the lateral boundaries of the domain, the difference fields may be spectrally decomposed into pure sine waves. The resulting spectra are evaluated separately for a large-scale part (with wavelength greater than 500 km) and a mesoscale part.

Figs. 10a to d show the mean over all 00 UTC-forecasts of July, 1991. At the beginning of the forecast, the mean difference of the wind component u ("zonal" wind) nearly vanishes but the root-mean-square (RMS) difference between the analyzed EM- and GM-values is nearly independent of height around 1.5 to 2.0 m/s. Large-scale and mesoscale structures contribute approximately the same amount to the total difference.

At the end of the EM-forecast (78 h), mean differences are still close to zero but the RMS-differences have grown to 2.5 to 4.5 m/s, with large values at the jet level. Whereas the mesoscale RMS-differences remain almost constant with time, the large-scale ones more than doubled. The growing large-scale differences between EM and GM can be interpreted as a drift of both models towards their specific model climate determined by the numerical and physical structure. Thus EM does not only add mesoscale detail to GM-forecasts but often exhibits differences in the large-scale.

The temporal evolution of the temperature difference between EM and GM (Figs. 11a to d) reveals a similar trend. Here the mean difference does not vanish and suggests a systematically warmer tropopause in EM in comparison with GM.

4.2 Verification against analyses

Tab. 3a and b present root-mean-square errors (RMS, left) and tendency correlations (right) for the previous operational model BKF (mesh size 254 km, 9 levels) and the models GM and EM for the months April and July, 1991. Each model is verified against its own analysis. A 48h-EM- (or GM-) forecast often has the same scores as a 24 to 36h-BKF-forecast; thus the quality of the operational forecasts at DWD improved

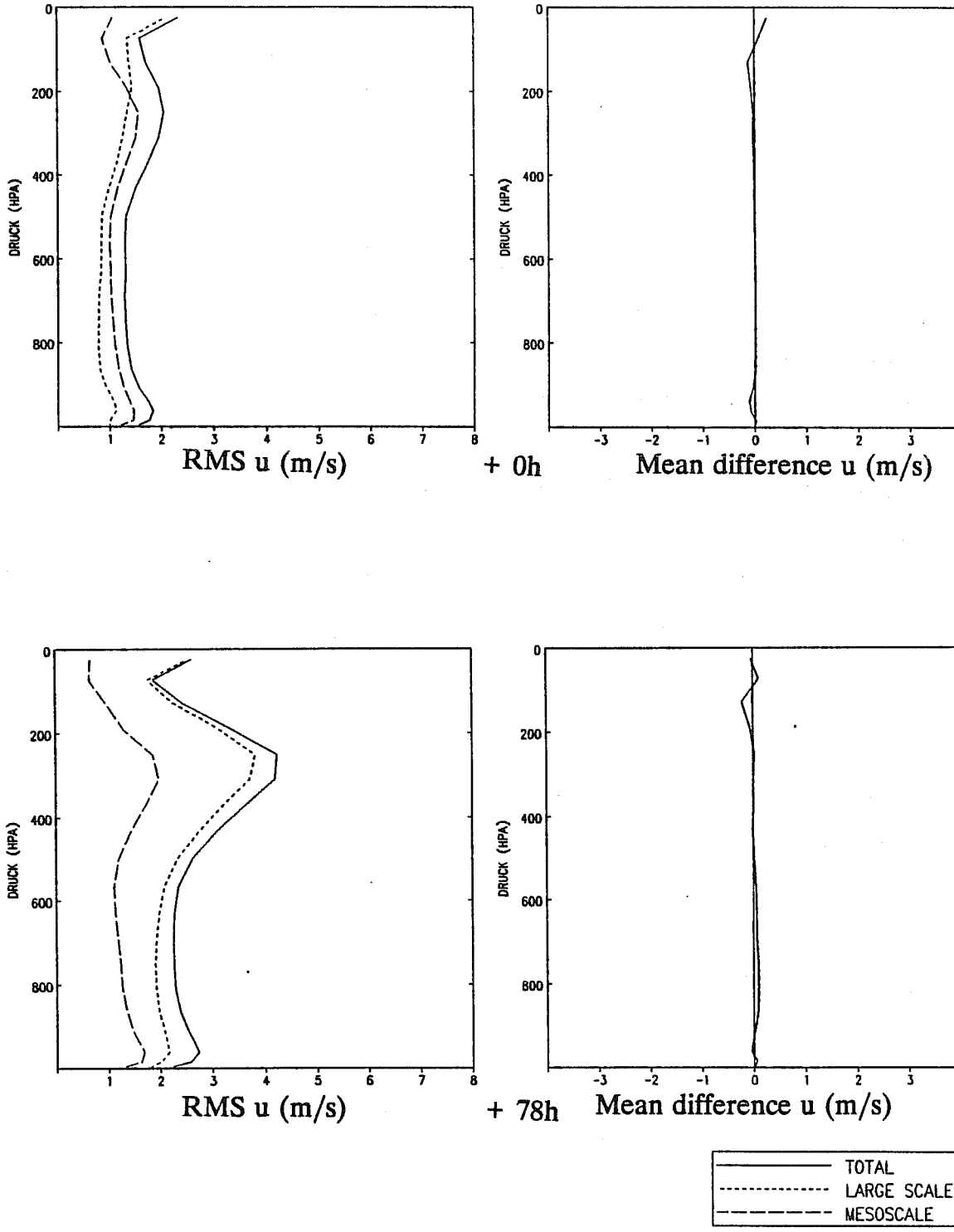

Fig. 10 Wind component u; difference between EM and GM;
mean of all 00 UTC-forecasts, July, 1991.
Top: Initialized analyses,
Bottom: 78h-forecasts,
Left: RMS-difference between EM and GM.
Right: Mean differences.

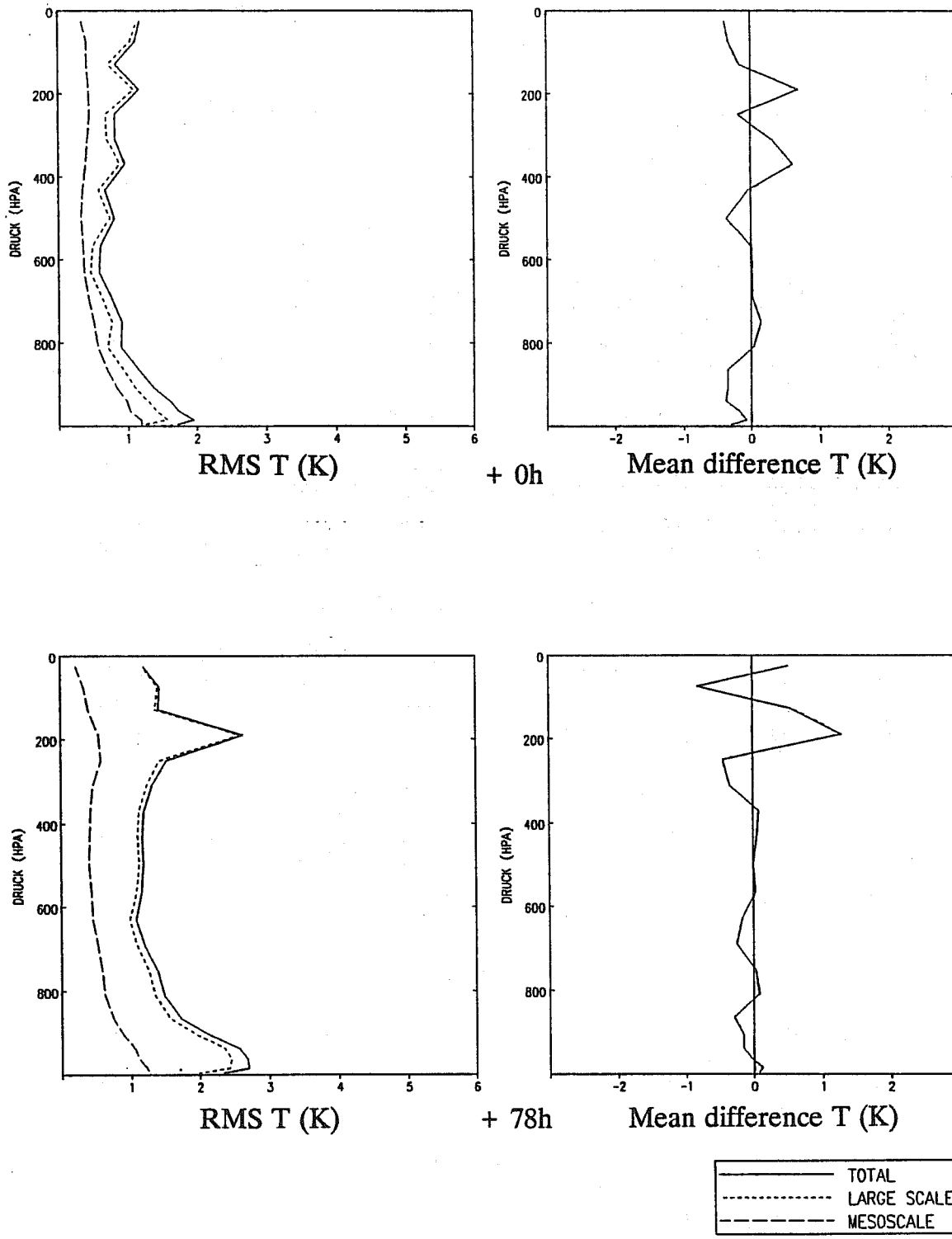

Fig. 11 Same as Fig. 10, but for temperature T.

RMS-Error | Tendency Correlation

Surface pressure (hPa)

Time	BKF	EM	GM	Time	BKF	EM	GM
+24h	2.545	1.814	1.876	+24h	0.937	0.969	0.967
+48h	4.422	3.168	3.185	+48h	0.881	0.940	0.938
+72h	6.217	4.726	4.659	+72h	0.801	0.896	0.898

Geopotential (gpm) at 500 hPa

Time	BKF	EM	GM	Time	BKF	EM	GM
+24h	22.147	16.616	16.221	+24h	0.950	0.974	0.977
+48h	40.978	30.942	29.540	+48h	0.915	0.958	0.963
+72h	61.152	48.007	46.020	+72h	0.861	0.927	0.934

Temperature (K) at 850 hPa

Time	BKF	EM	GM	Time	BKF	EM	GM
+24h	1.700	1.319	1.465	+24h	0.878	0.946	0.941
+48h	2.393	1.976	2.144	+48h	0.865	0.925	0.922
+72h	3.113	2.666	2.785	+72h	0.804	0.884	0.889

Temperature (K) at 500 hPa

Time	BKF	EM	GM	Time	BKF	EM	GM
+24h	1.285	1.029	1.039	+24h	0.924	0.957	0.959
+48h	1.973	1.694	1.679	+48h	0.896	0.932	0.937
+72h	2.746	2.379	2.377	+72h	0.835	0.889	0.896

Relative humidity (%) at 700 hPa

Time	BKF	EM	GM	Time	BKF	EM	GM
+24h	21.426	14.764	14.760	+24h	0.730	0.903	0.893
+48h	27.161	23.419	21.849	+48h	0.632	0.779	0.791
+72h	31.048	28.735	26.707	+72h	0.523	0.679	0.695

Winds (m/s) at 850 hPa

Time	BKF	EM	GM	Time	BKF	EM	GM
+24h	-	2.179	2.346	+24h	-	0.951	0.940
+48h	-	3.489	3.640	+48h	-	0.873	0.859
+72h	-	4.688	4.814	+72h	-	0.770	0.755

Winds (m/s) at 250 hPa

Time	BKF	EM	GM	Time	BKF	EM	GM
+24h	-	4.189	4.324	+24h	-	0.972	0.962
+48h	-	6.411	6.302	+48h	-	0.935	0.919
+72h	-	8.933	8.622	+72h	-	0.873	0.848

Tab. 3a Verification against analyses; Root-Mean-Square (RMS) and tendency correlation of BKF, EM, and GM.
Mean over April, 1991. Area: North Atlantic and Europe.

RMS-Error | Tendency Correlation

Surface pressure (hPa)

Time	BKF	EM	GM	Time	BKF	EM	GM
+24h	1.866	1.473	1.618	+24h	0.906	0.939	0.930
+48h	2.942	2.374	2.523	+48h	0.886	0.926	0.919
+72h	4.066	3.284	3.384	+72h	0.823	0.884	0.880

Geopotential (gpm) at 500 hPa

Time	BKF	EM	GM	Time	BKF	EM	GM
+24h	19.812	12.769	12.904	+24h	0.926	0.966	0.966
+48h	32.775	22.313	22.803	+48h	0.901	0.953	0.951
+72h	45.504	32.968	34.279	+72h	0.844	0.920	0.909

Temperature (K) at 850 hPa

Time	BKF	EM	GM	Time	BKF	EM	GM
+24h	1.454	1.259	1.342	+24h	0.809	0.879	0.869
+48h	2.032	1.818	1.951	+48h	0.818	0.864	0.855
+72h	2.502	2.304	2.468	+72h	0.775	0.822	0.809

Temperature (K) at 500 hPa

Time	BKF	EM	GM	Time	BKF	EM	GM
+24h	1.163	0.899	0.892	+24h	0.869	0.932	0.931
+48h	1.630	1.361	1.350	+48h	0.856	0.908	0.906
+72h	2.071	1.782	1.792	+72h	0.790	0.846	0.846

Relative humidity (%) at 700 hPa

Time	BKF	EM	GM	Time	BKF	EM	GM
+24h	18.208	11.755	11.001	+24h	0.670	0.902	0.893
+48h	21.983	19.183	16.898	+48h	0.615	0.783	0.792
+72h	24.004	23.415	20.678	+72h	0.566	0.687	0.702

Winds (m/s) at 850 hPa

Time	BKF	EM	GM	Time	BKF	EM	GM
+24h	-	1.878	2.050	+24h	-	0.936	0.924
+48h	-	2.732	2.933	+48h	-	0.861	0.840
+72h	-	3.499	3.812	+72h	-	0.770	0.721

Winds (m/s) at 250 hPa

Time	BKF	EM	GM	Time	BKF	EM	GM
+24h	-	4.103	4.211	+24h	-	0.961	0.944
+48h	-	6.135	6.270	+48h	-	0.910	0.870
+72h	-	7.920	8.185	+72h	-	0.847	0.769

Tab. 3b Verification against analyses; Root-Mean-Square (RMS) and tendency correlation of BKF, EM, and GM.
Mean over July, 1991. Area: North Atlantic and Europe.

considerably. EM has even slightly better scores than GM for some parameters, although the mesoscale flow pattern in the EM-analysis with its high variance and lower predictability tends to increase the RMS-error and to decrease the tendency correlation.

Figs. 12a to c show daily RMS-errors of surface pressure forecasts for the models BKF, GM, and EM from March to July, 1991. Probably as a result of the tuning efforts, EM is slightly better than GM at the surface since April 1991, but as visible in Fig. 13a to c, does not differ much in the geopotential at 500 hPa.

4.3 Verification against observations

The EM-forecasts of 2m-temperature, 10m-wind (speed and direction) and total cloudiness for 39 surface stations in Germany are verified against the corresponding observations. Figs. 14a, b, c and d show the mean errors for the four parameters, Figs. 15a, b, c, and d the percentage of EM-forecasts that were considered to be synoptically correct for July 1991. The mean errors exhibit a pronounced diurnal cycle: 2m-temperature is slightly higher than observed almost throughout the forecast period, especially early morning; 10m-winds are too strong in the night and too weak during daytime. The percentage of correct forecasts vary between almost 80 % for short range temperature forecasts and 50 % for cloud cover. The low number of correct forecasts of wind direction is misleading because the cases with weak and variable winds (< 2m/s) are not excluded from the sample.

Fig. 16 compares forecasts of the 2m-temperature for Frankfurt (Airport) made by three models (BKN, which is a limited area version of BKF with 9 layers and a mesh size of 127 km, GM and EM) with three-hourly observations. Two forecast ranges, 12-36 h, and 36-60 h, are considered. A mean over 25 days from 7 to 31 August 1991, of all 00 UTC-forecasts was taken. The period is characterized mostly by a strongly anticyclonic regime over Central Europe with almost no clouds. But even then substantial differences exist between the mean diurnal cycles (Figs. 16a and c) of the models and the local observation. Comparing the results, one has to keep in mind that the difference between model and reality does not only reflect model errors, but also the influence of very small-scale effects characteristic of the local site of observation, which is not necessarily representative of a larger area. Figs. 16b and d show the RMS-errors and indicate that there is still room for improvement in the local weather forecast even for such "simple" types of weather.

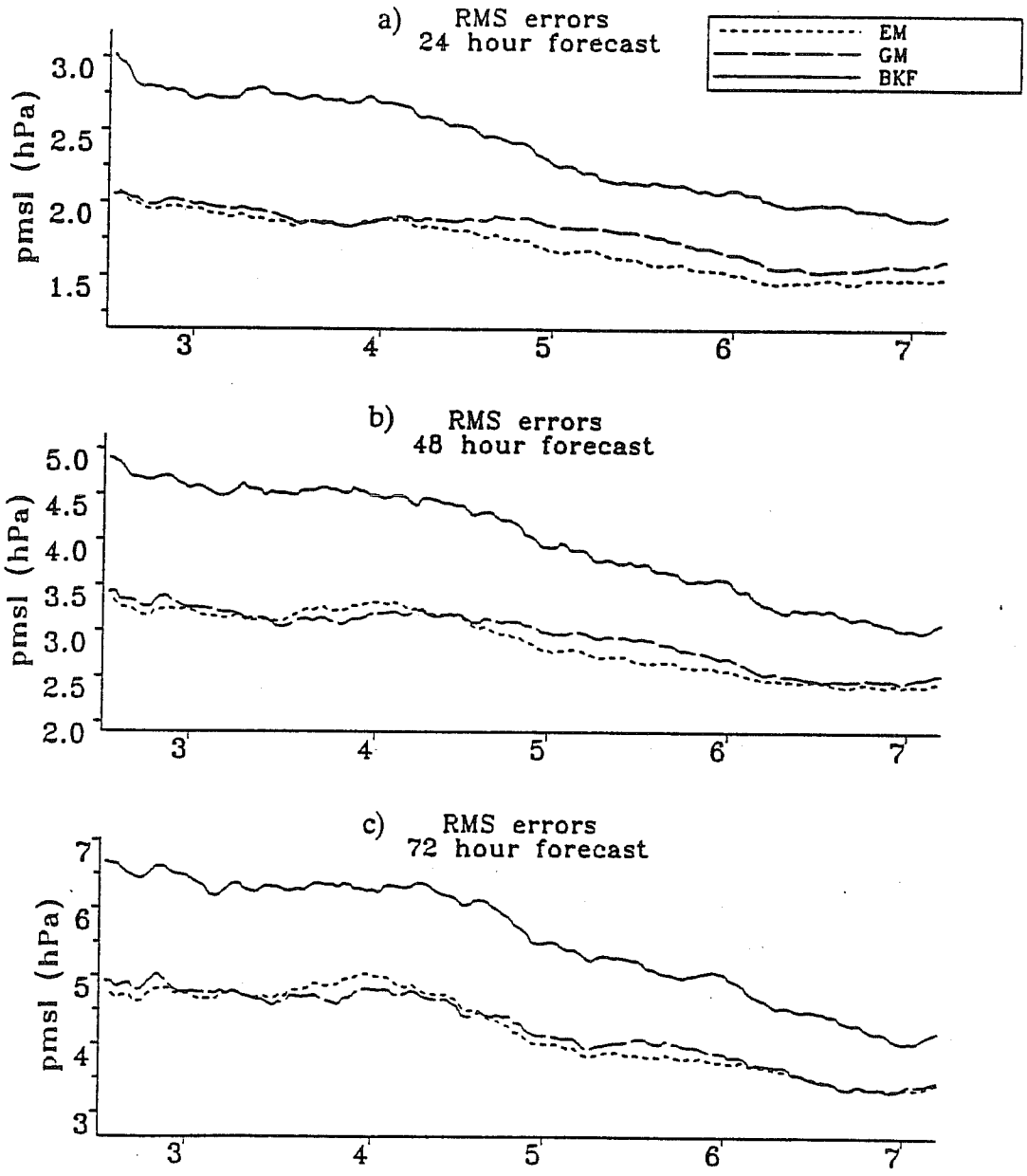

Fig. 12 Root-Mean-Square (RMS)-errors of surface pressure forecasts for the models EM, GM, BKF. 30 day running mean; February - July, 1991. Area: North Atlantic and Europe.

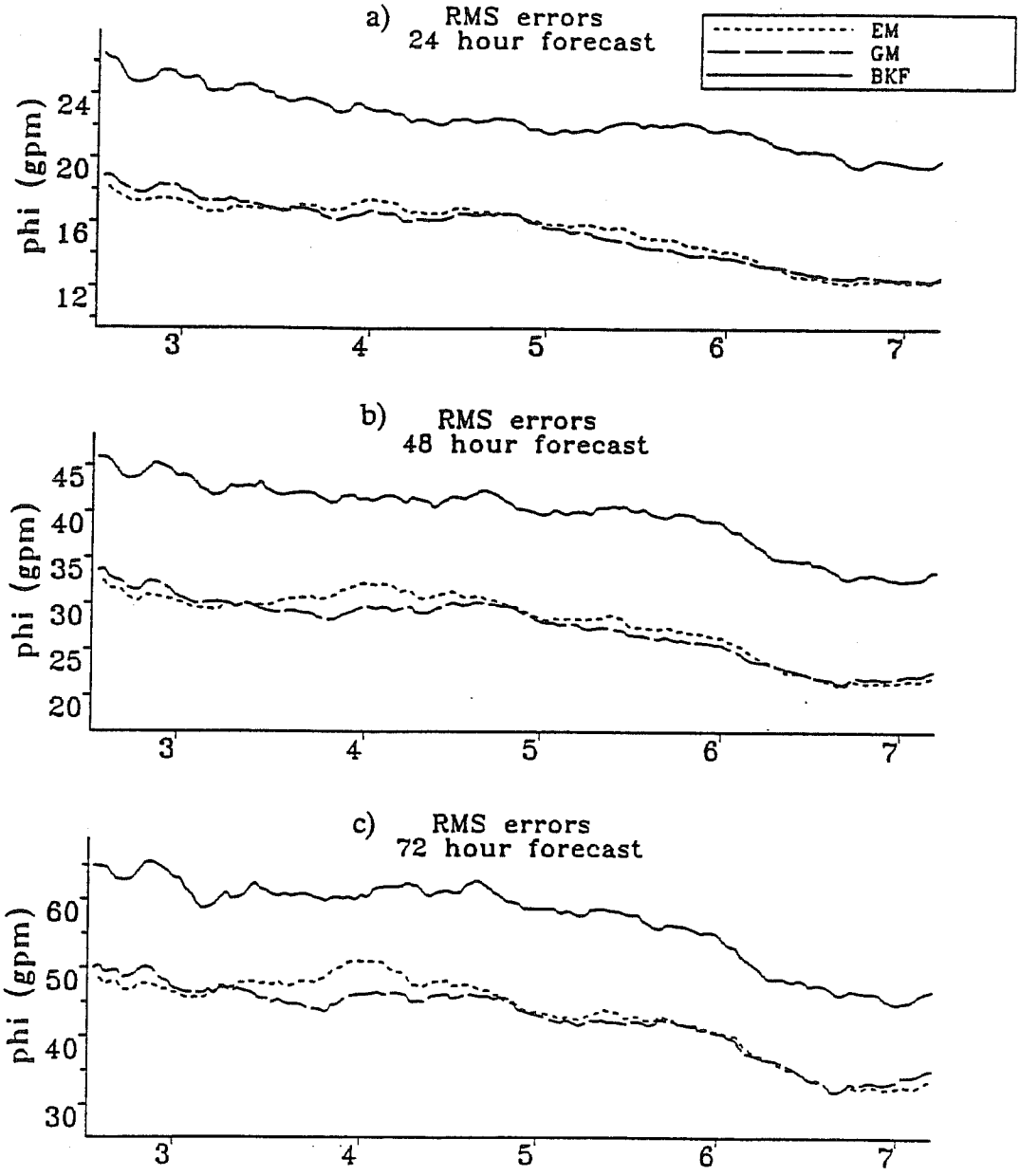

Fig. 13 Same as Fig. 12, but for geopotential at 500 hPa.

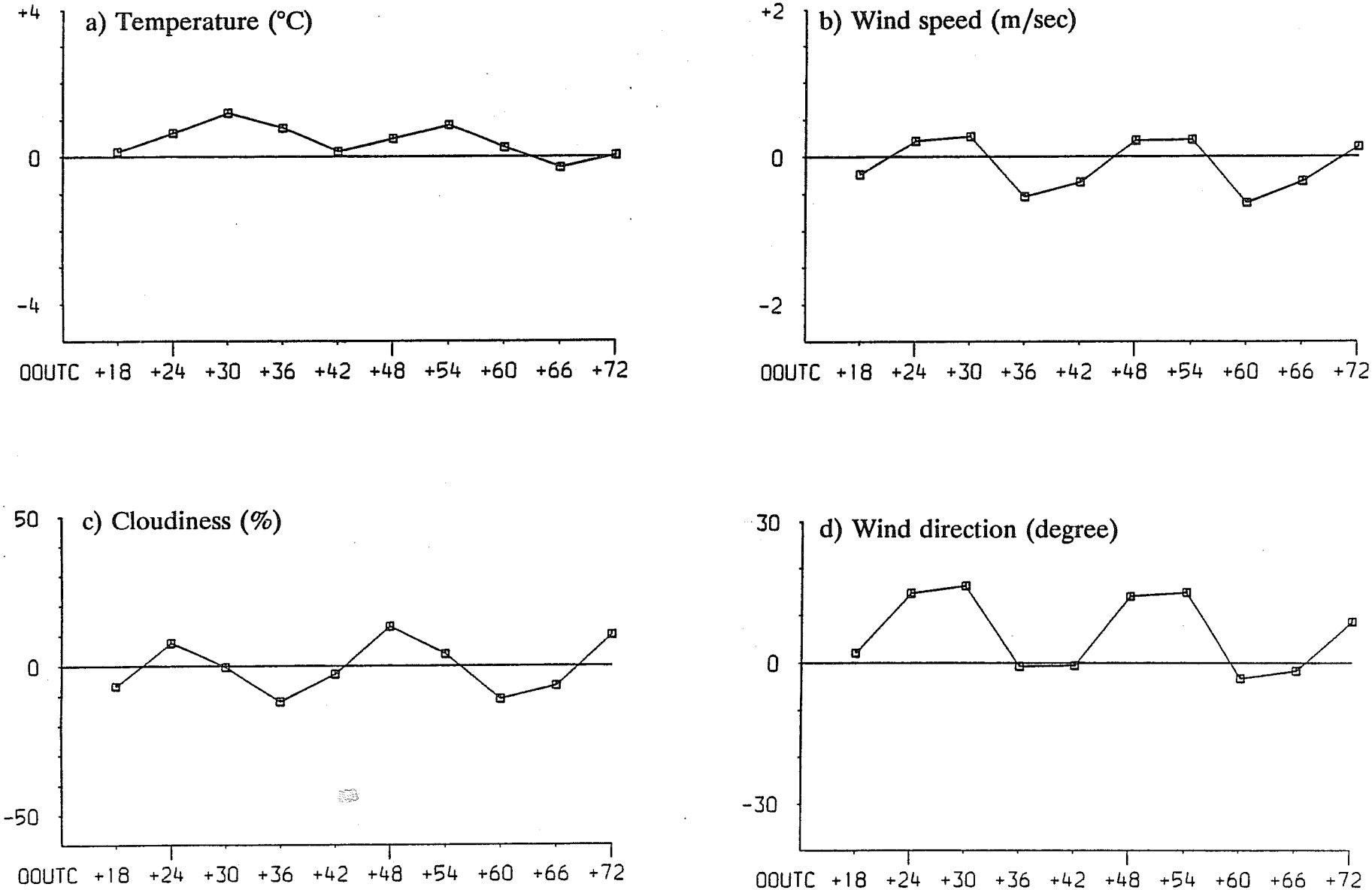

Fig. 14 Verification of EM-forecasts for 39 stations in Germany:
Mean errors for July, 1991.

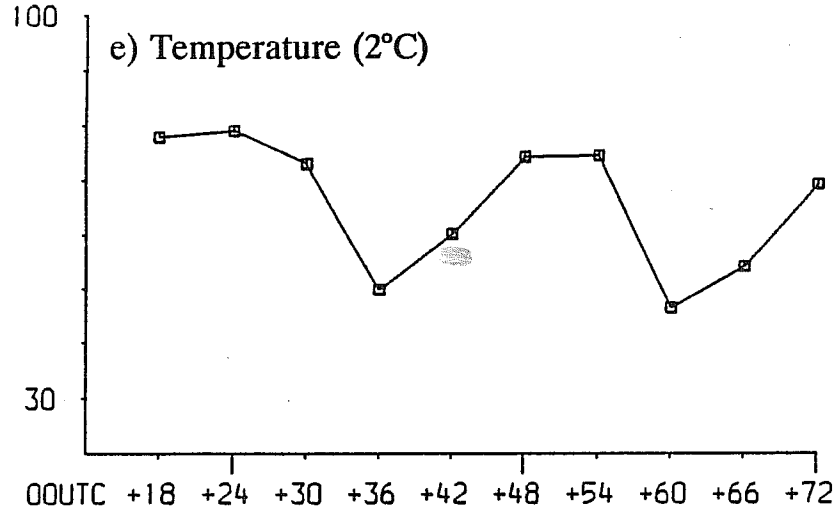

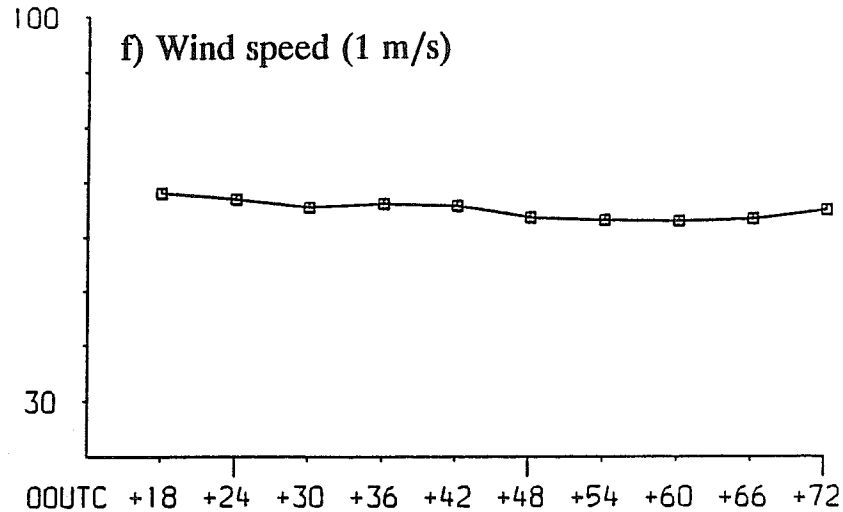

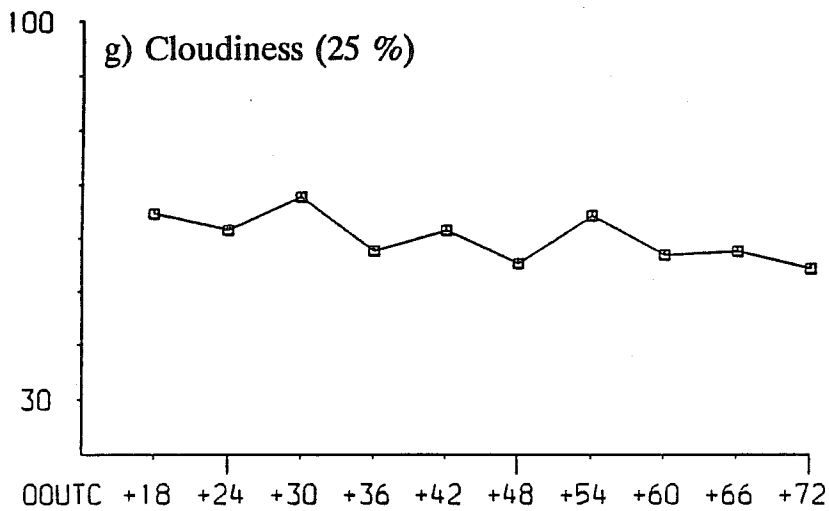

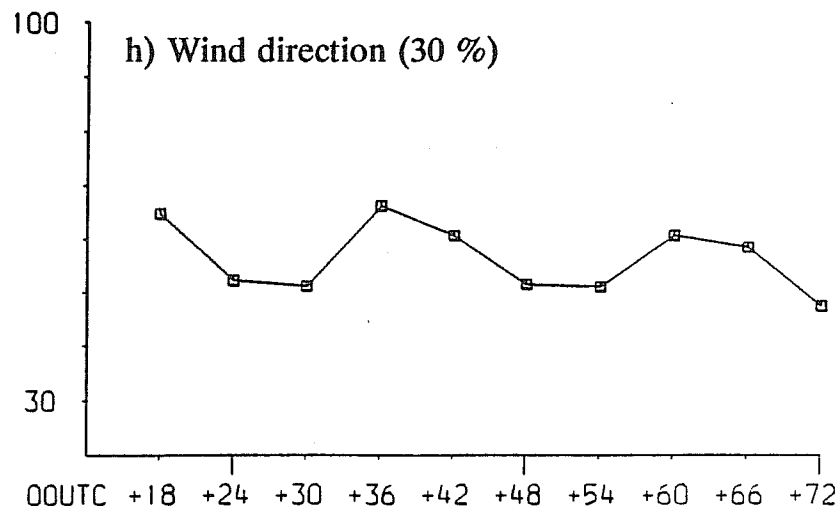

Fig. 15 Verification of EM-forecasts for 39 stations in Germany: Percentage of correct forecasts (i.e. with errors less than the number indicated in brackets) for July, 1991.

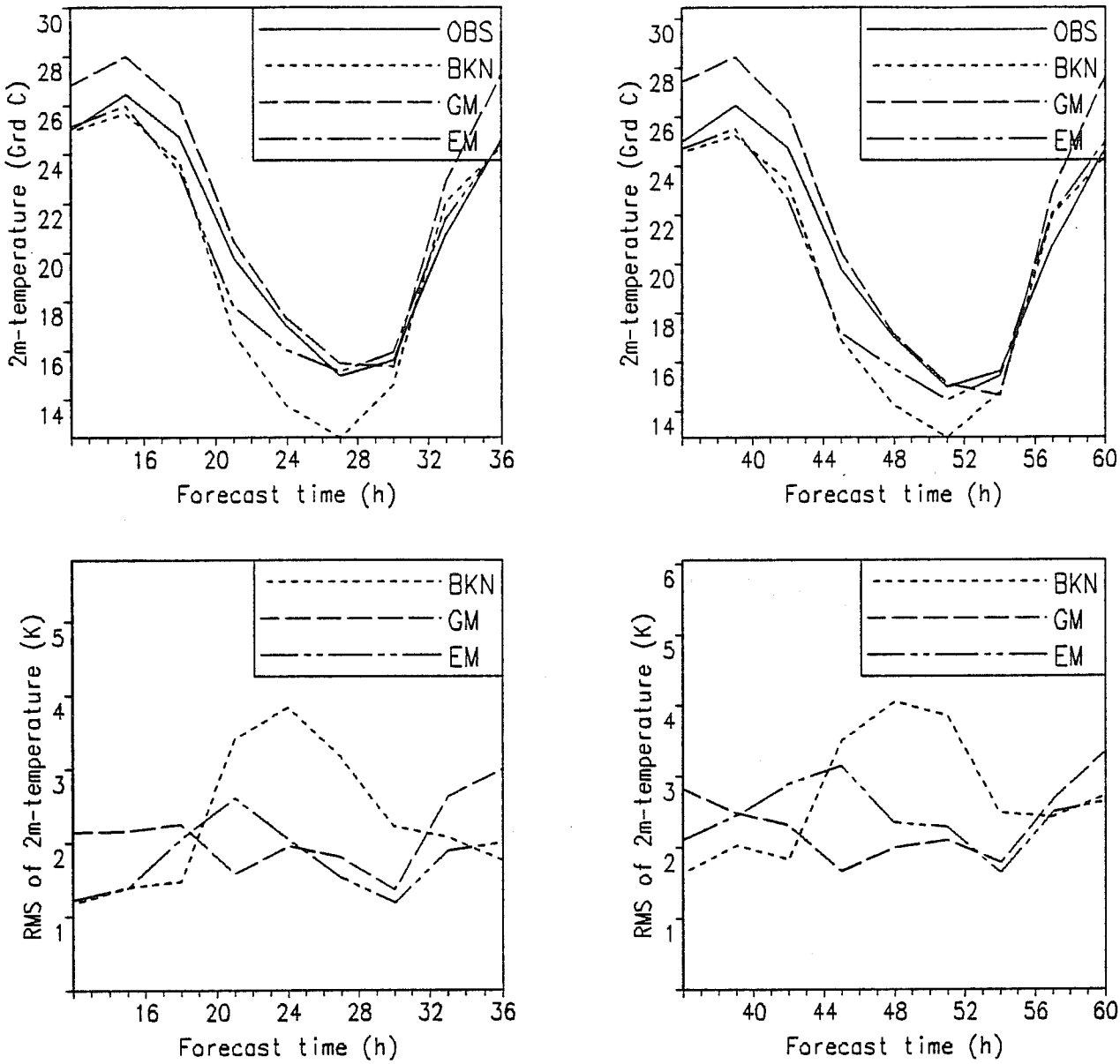

Fig. 16 Top: Mean diurnal cycle of 2m-temperature at Frankfurt (Airport); 7 - 31 August, 1991.
Observation (solid line) and three model forecasts starting 00 UTC.
Left: Time range: 12 - 36h,
right: Time range: 36 - 60h.

Bottom: RMS-error of 2m-temperature forecasts of the three models.
Left: Time range: 12 - 36h,
right: Time range: 36 - 60h.

5. OUTLOOK

After the implementation of the new model chain consisting of the Global-Modell (GM) and the Europa-Modell (EM), most efforts are concentrated on tuning and improving EM. Especially the development of suitable tools for checking the validity and limits of EM's parameterization schemes is necessary.

At the same time, the third link of the model chain, the high-resolution model (DM), will be developed in close cooperation with the Swiss Meteorological Agency. Here much work on numerical aspects has to be done, e.g. on semi-Lagrangian and positive-definite advection schemes.

6. ACKNOWLEDGEMENTS

Thanks are due to all members of the research department of DWD, especially to those who helped directly in developing the EM. I am greatly indepted to G. Doms for the close cooperation during the development of the adiabatic part of the model, to E. Heise, who is responsible for the physical parameterizations, and to D. Skalischus for speeding-up the model. M. Pfaendtner took care of the manuscript.

7. LITERATURE

Davies, H.C., 1976: A lateral boundary formulation for multi-level prediction models. Quart. J. R. Meteor. Soc., 102, 405-418.

Doms, G., 1990: Some physical/numerical aspects of the Europa-Modell. LAM Newsletter No. 19, 187-199.

Jacobsen, I. and E. Heise, 1982: A new economic method for the computation of the surface temperature in numerical models. Beitr. Phys. Atm., 55, 128-141.

Lorenc, A., 1981: Design of ECMWF analysis scheme. Seminar 1980, Data Assimilation Methods, ECMWF, Reading, U.K., 83-106.

Louis, J.-F., 1979: A parametric model of vertical eddy fluxes in the atmosphere. Boundary-Layer Meteor., 17, 187-202.

Majewski, D., 1985: Balanced initial and boundary values for a limited-area model. Beitr. Phys. Atm., 58, 147-159.

Majewski, D., 1990: On the influence of lateral boundary values on limited area forecasts. LAM Newsletter No. 19, 200-206.

Mellor, G.L. and T. Yamada, 1974: A hierarchy of turbulence closure models for planetary boundary layers. J. Atmos. Sci., 31, 1791-1806.

Müller, E., 1981: Turbulent flux parameterization in a regional-scale model. ECMWF Workshop on planetary boundary layer parameterization, 193-220.

Simmons, A.J. and D.M. Burridge, 1981: An energy and angular-momentum conserving vertical finite-difference scheme and hybrid vertical coordinates. Mon. Wea. Rev., 109, 758-766.

Temperton, C., 1988: Implicit normal mode initialization. Mon. Wea. Rev., 116, 1013-1031.

8. APPENDIX

The equations of motions for a rotated spherical coordinate system (λ', φ') are identical to those for the usual geographic coordinates (λ, φ) except that the Coriolis parameter depends on the latitude and longitude of the rotated grid. For simplicity, λ' and φ' are written λ and φ.

8.1 List of symbols

a: Radius of the earth (a = 6371229 m)

c_P: Specific heat of dry air at constant pressure (c_P=1005 J/(kg K))

E^w: Saturation pressure of water vapor

F_H^{ψ}: Horizontal diffusion term of quantity ψ (u, v, h, q_w)

f: Coriolis parameter (Eq. A.07)

g: Constant of gravity (g = 9.80665 m/s^2)

h: Specific total heat content

K: Specific kinetic energy

L: Latent heat of condensation (L = 2.501 10^6 J/kg)

p: Pressure

p_s: Surface pressure at the height of the orography

Q_v^s: Specific water vapor content at saturation

q_c: Specific cloud water content

q_v: Specific water vapor content

q_w: Specific total water content

R: Gas constant of dry air (R = 287.05 J/(kg K))

R_v: Gas constant of water (R_v= 461.51 J/(kg K))

T: Temperature

T_v: Virtual temperature

t: Time

u: Wind component in "zonal" direction of the rotated grid

v: Wind component in "meridional" direction of the rotated grid

α: Specific volume (Eq. A.13)

ζ: Vertical component of relative vorticity

η: Hybrid vertical coordinate

$\dot{\eta}$: Vertical velocity in the η-system

η_p: Vertical turbulent flux of total heat

η_q: Vertical turbulent water flux

λ: Rotated longitude

λ_N: Geographic longitude of rotated north pole

μ_R: Boundary relaxation coefficient

τ_λ: Vertical turbulent flux of "zonal" wind

τ_φ: Vertical turbulent flux of "meridional" wind

φ: Rotated latitude

φ_N: Geographic latitude of rotated north pole

ψ_R: Boundary value of the prognostic quantity (u, v, h, q_w, p_s)

$\left(\frac{\partial \psi}{\partial t}\right)_s$ Local time change of ψ due to subgrid-scale processes (except vertical and horizontal diffusion)

Ω: Angular velocity of the earth (Ω = 7.292 10^{-5} s^{-1})

ω: Vertical velocity in the pressure system

8.2 Continuity equation

$$\frac{\partial}{\partial \eta}\left(\frac{\partial p}{\partial t}\right) + \frac{1}{a\cos(\varphi)}\left\{\frac{\partial}{\partial \lambda}\left(u\frac{\partial p}{\partial \eta}\right) + \frac{\partial}{\partial \varphi}\left(v\cos(\varphi)\frac{\partial p}{\partial \eta}\right)\right\} + \frac{\partial}{\partial \eta}\left(\dot{\eta}\frac{\partial p}{\partial \eta}\right) = - \mu_R\left(\frac{\partial p}{\partial \eta} - \frac{\partial p_R}{\partial \eta}\right) \qquad \text{A.01}$$

The r.h.s.-term forces the EM-forecast to follow closely the GM-forecast in the boundary zone.

Integrating Eq. A.01 from η=0 to η=1 with the boundary conditions $\dot{\eta}$=0 at η=0 and η=1 yields the equation of the surface pressure tendency.

8.3 Surface pressure tendency

$$\frac{\partial p_S}{\partial t} = - \frac{1}{a\cos(\varphi)} \int_0^1 \left\{\frac{\partial}{\partial \lambda}\left(u\frac{\partial p}{\partial \eta}\right) + \frac{\partial}{\partial \varphi}\left(v\cos(\varphi)\frac{\partial p}{\partial \eta}\right)\right\} d\eta - \mu_R (p_S - p_{SR}) \qquad \text{A.02}$$

Integrating Eq. A.01 from η=0 to $\eta=\eta_{k+1/2}$ yields the equation for the vertical velocity in the η-system at the level k+1/2.

8.4 Vertical velocity in the η-system

$$\left(\dot{\eta}\,\frac{\partial p}{\partial \eta}\right)_{k+1/2} = -\left(\frac{\partial p}{\partial p_S}\right)_{k+1/2}\left\{\frac{\partial p_S}{\partial t} + \mu_R(p_S - p_{SR})\right\}$$

$$-\frac{1}{a\cos(\varphi)}\int_0^{\eta_{k+1/2}}\left\{\frac{\partial}{\partial \lambda}\left(u\frac{\partial p}{\partial \eta}\right) + \frac{\partial}{\partial \varphi}\left(v\cos(\varphi)\frac{\partial p}{\partial \eta}\right)\right\}d\eta \qquad \text{A.03}$$

8.5 Equation of the u-component

$$\frac{\partial u}{\partial t} - \frac{1}{\cos(\varphi)}Q\frac{\partial p}{\partial \eta}v\cos(\varphi) + \frac{1}{a\cos(\varphi)}\frac{\partial}{\partial \lambda}(\Phi + K) +$$

$$\frac{RT_V}{a\cos(\varphi)}\frac{\partial}{\partial \lambda}[\ln(p)] + \dot{\eta}\frac{\partial u}{\partial \eta} = F_H{}^u - g\left(\frac{\partial p}{\partial \eta}\right)^{-1}\frac{\partial \tau_\lambda}{\partial \eta} + \left(\frac{\partial u}{\partial t}\right)_S - \mu_R(u - u_R) \qquad \text{A.04}$$

Q, K, f, Φ, and T_v follow from:

$$Q = \frac{\zeta + f}{\partial p/\partial \eta} = \left(\frac{\partial p}{\partial \eta}\right)^{-1}\left\{f + \frac{1}{a\cos(\varphi)}\left(\frac{\partial v}{\partial \lambda} - \frac{\partial}{\partial \varphi}[u\cos(\varphi)]\right)\right\} \qquad \text{A.05}$$

$$K = \frac{1}{2}\left(u^2 + \frac{1}{\cos(\varphi)}v^2\cos(\varphi)\right) \qquad \text{A.06}$$

$$f = 2\,\Omega\left[\sin(\varphi_N)\sin(\varphi) + \cos(\varphi_N)\cos(\varphi)\cos(\lambda)\right] \qquad \text{A.07}$$

$$\frac{\partial \Phi}{\partial \eta} = -\frac{R\,T_V}{p}\frac{\partial p}{\partial \eta} \qquad \text{A.08}$$

$$T_V = T\left(1 + \left(\frac{R_V}{R} - 1\right)q_V\right) \qquad \text{A.09}$$

8.6 Equation of the v-component

$$\frac{\partial v}{\partial t} + Q\frac{\partial p}{\partial \eta}u + \frac{1}{a}\frac{\partial}{\partial \varphi}(\Phi + K) +$$

$$\frac{RT_V}{a}\frac{\partial}{\partial \varphi}[\ln(p)] + \dot{\eta}\frac{\partial v}{\partial \eta} = F_H{}^v - g\left(\frac{\partial p}{\partial \eta}\right)^{-1}\frac{\partial \tau_\varphi}{\partial \eta} + \left(\frac{\partial v}{\partial t}\right)_S - \mu_R(v - v_R) \qquad \text{A.10}$$

8.7 Equation of the specific total heat

$$\frac{\partial h}{\partial t} + \frac{1}{a\cos(\varphi)}\left[u\frac{\partial h}{\partial \lambda} + v\cos(\varphi)\frac{\partial h}{\partial \varphi}\right] + \dot{\eta}\frac{\partial h}{\partial \eta} =$$

$$\alpha\,\omega + F_H{}^h - g\left(\frac{\partial p}{\partial \eta}\right)^{-1}\frac{\partial \eta_p}{\partial \eta} + \left(\frac{\partial h}{\partial t}\right)_S - \mu_R(h - h_R) \qquad \text{A.11}$$

h is defined as: $h = c_p T + L q_V$ A.12

The specific volume follows from the ideal gas law:

$$p\,\alpha = RT_V \qquad \text{A.13}$$

8.8 Energy conversion

$$(\alpha\,\omega)_k = (RT_V)_k\left(\frac{\omega}{p}\right)_k \qquad \text{A.14}$$

with:

$$\left(\frac{\omega}{p}\right)_k = \frac{1}{p_k}\left\{-\left(\frac{\partial p}{\partial p_S}\right)_k \mu_R(p_S - p_{SR})\right\} -$$

$$\frac{1}{p_k}\left\{\frac{1}{a\cos(\varphi)}\int_0^{\eta_k}\left[\frac{\partial}{\partial \lambda}\left(u\frac{\partial p}{\partial \eta}\right) + \frac{\partial}{\partial \varphi}\left(v\cos(\varphi)\frac{\partial p}{\partial \eta}\right)\right]d\eta\right\} + \qquad \text{A.15}$$

$$\frac{1}{a\cos(\varphi)}\left\{u\frac{\partial}{\partial \lambda}[\ln(p)] + v\cos(\varphi)\frac{\partial}{\partial \varphi}[\ln(p)]\right\}_k$$

It is important to note that in this equation the influence of the boundary values (index R) does not cancel as in Eq. A.03 for the vertical velocity in the η-system.

8.9 Equation of the specific total water content

$$\frac{\partial q_W}{\partial t} + \frac{1}{a\cos(\varphi)}\left[u\frac{\partial q_W}{\partial \lambda} + v\cos(\varphi)\frac{\partial q_W}{\partial \varphi}\right] + \dot{\eta}\frac{\partial q_W}{\partial \eta} =$$

$$F_H{}^q - g\left(\frac{\partial p}{\partial \eta}\right)^{-1}\frac{\partial \eta_q}{\partial \eta} + \left(\frac{\partial q_W}{\partial t}\right)_S - \mu_R(q_W - q_{WR}) \qquad \text{A.16}$$

with $$q_W = q_V + q_C \qquad \text{A.17}$$

8.10 Completing the system of the equations of the EM

The five prognostic equations (A.02, A.04, A.10, A.11, A.16) and nine diagnostic relations (A.03, A.05, A.06, A.08, A.09, A.12, A.13, A.14, A.17) form the set of equations for the five prognostic (u, v, h, q_w, p_s) and ten diagnostic quantities ($\dot{\eta}$, Q, K, T_v, Φ, ω, T, q_v, q_c, p). Thus one diagnostic equation is needed to complete the system of equations. The closure assumption is that inside of clouds there is saturation over water; i.e.:

$$q_V = Q_V{}^S(T,p) \qquad \text{A.18}$$

$Q_V{}^S$ is the specific water vapor content at saturation over water and is defined as:

$$Q_V{}^S(T,p) = \frac{R}{R_V}\frac{E^W(T)}{p - \left(1 - \frac{R}{R_V}\right)E^W(T)} \qquad \text{A.19}$$

The saturation pressure follows from Magnus' formula:

$$E^W(T) = B1\exp\left(B2W\frac{T - B3}{T - B4W}\right) \qquad \text{A.20}$$

with the constants:

B1 = 610.78 Pa

B2W = 17.2693882

B3 = 273.16 K

B4W = 35.86 K

Using A.18, A.19, and A.20, the diagnostic quantities T, q_v, and q_c can be derived from the prognostic quantities h and q_w under the assumption of saturation over water inside of clouds distinguishing between cloud and no-cloud cases:

Clouds: $q_V = Q_V^S(T,p)$ and $q_C = q_W - Q_V^S(T,p)$ A.21

No-clouds: $q_V = q_W$ and $q_C = 0$ A.22

The partitioning has to be done iteratively, usually one to three iterations are needed.